Spring 4-23-2021

The analysis of groundwater recharge in Mongolia using vadose zone modeling

Khulan Batsukh
University of Nebraska-Lincoln, kbatsukh2@huskers.unl.edu

THE ANALYSIS OF GROUNDWATER RECHARGE IN MONGOLIA USING VADOSE ZONE MODELING

by

Khulan Batsukh

A THESIS

Presented to the Faculty of

The Graduate College at the University of Nebraska

In Partial Fulfillment Requirements

For the Degree of Master of Science

Major: Earth and Atmospheric Sciences

Advisors: Professor Vitaly A.Zlotnik

Professor Erin Haacker

Lincoln, Nebraska

May, 2021

THE ANALYSIS OF GROUNDWATER RECHARGE IN MONGOLIA USING VADOSE ZONE MODELING

Khulan Batsukh, M.S.

University of Nebraska, 2021

Advisors: Vitaly A.Zlotnik and Erin Haacker

Knowledge of groundwater recharge (*GR*) is vital for optimal water resources management under an arid continental climate. However, in vast territories such as Mongolia, direct measurements of *GR* are unfeasible because they mandate excessive costs, stemming from time-consuming and labor-demanding efforts. A valid alternative to direct measurements is numerical models based on the monitoring of precipitation (*P*) and evapotranspiration (*ET*) for simulating *GR*. While direct measurements of *ET* are logistically problematic and unpractical for large-scale applications, a reliable prediction may be derived from crop reference evapotranspiration (ET_0) which is calculable from limited data and will feed numerical models to evaluate a (pseudo) realistic *GR* as output. The crop reference evapotranspiration (ET_0) was calculated employing the Hargreaves (Har) temperature-based ET_0 method that closely simulated the internationally recognized standard FAO Penman-Monteith (FAO-56 PM) method (calculated with available data at limited locations). The set of weather data required for FAO-56 PM is still mostly unavailable or not easily accessible in data-limited countries such as Mongolia. The Har temperature-based method showed good potential to replace FAO-56 PM in the region according to our analysis. A time-variable and spatially-variable crop coefficient (K_c) was used to convert Har ET_0 into a biome-specific potential evapotranspiration (ET_p) for 41

study locations. However, there were no readily available estimates of K_c in natural vegetation specific to Mongolia. A dynamic (time-variable) radiation-dependent (in Gobi Desert) or *LAI*-dependent (in steppe) K_c was adopted from the literature and used for the first time in Mongolia. The *LAI* dependent K_c was also adjusted due to the climate features of the region. The developed K_c values are important to convert ET_0 to ET_p with consideration of region's climate and any factors affecting the vegetation. The mean annual ET_0 ranged from 685 mm to 1129 mm, while the ET_p ranged from 147 mm to 695 mm. The *GR* rates were calculated using the estimated ET_p as input in the HYDRUS-1D numerical vadose zone model for 41 study locations across Mongolia. The mean annual *GR* rates were smaller than 12 mm in study locations and the *GR* tends to decrease when vegetation cover increases.

Table of contents

THE ANALYSIS OF GROUNDWATER RECHARGE IN MONGOLIA USING VADOSE ZONE MODELING ii
List of abbreviations x
Acknowledgements 1
CHAPTER 1. INTRODUCTION 3
Study locations 5
CHAPTER 2. SELECTION OF EVAPOTRANSPIRATION METHOD 8
Introduction 8
Methods 12
Determining the duration of the time series for simulation ET parameters 12
Approaches to ET estimation 13
Crop coefficients, K_c 15
Evaporation and Transpiration 20
The FAO Aridity Index, *AI* 21
Data collection 22
Temperature 22
Leaf Area Index, *LAI* 23
Results and discussion 26
The method selection for reference crop evapotranspiration, ET_0 26
Reference crop evapotranspiration results 30
Prediction of biome-specific potential evapotranspiration, ET_p 32
Conclusions 38
CHAPTER 3. THE ANALYSIS OF GROUNDWATER RECHARGE 39
Introduction 39
Methods 42
Modeling groundwater recharge using HYDRUS-1D 42
Pedotransfer functions 43
Net precipitation 44
Root water uptake 45
Comparing Groundwater recharge with existing groundwater recharge map 46
Vadose zone lag time 47

Data collection 49
Biome-specific potential Evapotranspiration 49
Soil hydraulic parameters 49
Root zone 50
Soil moisture 51
Depth to the water table 52
HYDRUS-1D setup 53
The HYDRUS-1D configuration 53
Setting initial condition and spin-up 54
Results and discussion 58
Actual evapotranspiration result, ET_a 58
Groundwater recharge rates 60
Calculating vadose zone lag time 67
Conclusions 68
CHAPTER 4. UNCERTAINTY AND CONCLUSIONS 69
Uncertainty 69
Conclusions 71
References 73
Appendices 80

List of Tables

Table 2.1. Previous ET studies in Mongolia 9
Table 2.2. FAO-56 PM, Har and Tho equations with required input data 13
Table 2.3. Categorization of natural zones 16
Table 2.4. Macro-classes and classes of the FAO *AI* 21
Table 2.5. Data sources 22
Table 2.6. Pearson correlation coefficients between FAO-56 PM ET_0 and meteorological variables over the ten weather stations in Mongolia 26
Table 2.7. Annual sums of ET_0 over the 41 weather stations in Mongolia 30
Table 2.8. 5-year annual average sums of water fluxes over 41 weather stations in Mongolia 33
Table 3.1. Data sources 49
Table 3.2. The main parameters of study locations 55
Table 3.3. Texture and *AI* class 56
Table 3.4. *GR* and *P* (mm/year) 61
Table 4.1. Uncertainties in study 69

List of Figures

Figure 1.1. Schematic overview of the two steps to model ground water recharge (GR) involving a) estimation of reference evapotranspiration (ET_0) from basic weather data obtained employing three different estimates (FAO56-PM, HAR, and Tho) and (b) modeling process that starts with obtaining potential evapotranspiration (ET_p) and crop coefficient (K_c) and leaf area index (LAI) as the inputs to of a hydrological model that generates values of ground water recharge (GR). 5
Figure 1.2. Locations of 41 weather stations (represented by the triangle symbol) on DEM (Digital Elevation Model) map retrieved from the Shuttle Radar Topography Mission (SRTM) in Mongolia (Earth Resources Observation And Science center, 2017). The ten blue triangles indicate the weather stations with a complete set of meteorological data used to compare FAO56-PM with temperature-based equations. 7
Figure 2.1. The mean precipitation and temperature /average of all available stations data/ 12
Figure 2.2. LAI_{dense} and A_{cm} values depending on *LAI*. 19
Figure 2.3. The comparison of daily temperature measurements in Khatgal 23
Figure 2.4. Map showing the monthly mean *LAI*s in the growing season, extracted from the dataset by (Mao & Yan., 2019). 25
Figure 2.5. Model performance indicators comparing the FAO-56 PM with Har (blue line) and Tho (red line) to estimate daily values of ET_0: (a) *RMSE* (mm d^{-1}) values and (b) values of R^2 (-) for ten weather stations. 27
Figure 2.6. Comparison between FAO-56 PM-based and temperature-based equations (Har ET_0 values are represented by blue circles and Tho ET_0 values are depicted by red circles) for predicting daily values of ET_0 at (a) Khatgal weather station, and b) Tsogtovoo weather station. 28
Figure 2.7. Annual average ET_0 calculated with FAO56-PM (blue bars), Har (orange bars), and Tho (gray bars) for ten weather stations in Mongolia. 29
Figure 2.8. The annual mean spatial FAO-56 PM ET_o map by FAO (2009) with corresponding Har ET_o values. The plot on the right shows the comparison between FAO-56 PM ET_o and Har ET_o. Diagonal dashed line depicts the identity line (1:1 line). 32
Figure 2.9. Annual average sums of E_p (white bars) and T_p (gray bars) and annual average *LAI* (orange line) over the 41 weather stations in Mongolia. 34
Figure 2.10. Calculated *AI* values obtained over the 41 weather stations compared to the aridity map (FAO-UN AI) extracted from the Global Aridity map (FAO-UN, 2015). The plot on the right shows the comparison between FAO-UN *AI* and Har *AI*. The diagonal dashed line depicts the identity line (1:1 line). 35
Figure 2.11. Maps showing the a) mean annual temperature and b) mean annual precipitation in study locations on DEM (Digital Elevation Model) map from SRTM (Earth Resources Observation And Science center, 2017). 35
Figure 2.12.Annual average sums of ET_0 and ET_p with *AI*. Weather stations are grouped in the Gobi Desert and steppe zones 36

Figure 2.13. Relationships between a) aridity index, *AI* and the ratio of ET_p over ET_0, and b) leaf area index, *LAI*, and the ratio of E_p over ET_p. Solid black lines represent linear regression equations reported with associated R^2. Vertical dashed lines delimit in a) plot delimit climate classes (arid and semi-arid). The data over the 41 weather stations are grouped in Gobi Desert (yellow circles) and steppe (green circles). 37
Figure 3.1. Schematic of the plant water stress function, $\alpha(\psi)$ by (Feddes, 1978) 46
Figure 3.2. Soil moisture at the bottom spin ups 57
Figure 3.3. Overall ET results in study locations 58
Figure 3.4.Trends in mean annual ET_a and *LAI*, and *AI* 59
Figure 3.5. Comparison of values of actual annual ET_a obtained from HYDRUS-1D one-dimensional soil-water balance method prepared by FAO (FAO, 2009a) on the map with a spatial resolution of 5 arc minutes. 60
Figure 3.6. Precipitation, evapotranspiration, and groundwater recharge (mm/year), obtained from Hargreaves equation for ET_p and reduced K_c 61
Figure 3.7. The *LAI* vs. *GR* in study locations 64
Figure 3.8. Relationship between *GR* rates and soil texture as a fraction of sand (%), silt (%), and clay (%). 65
Figure 3.9. The mean annual GR rates in study locations 65
Figure 3.10. Our mean annual *GR* results on the Renewable Groundwater Resource map by (Jadambaa et al., 2012, Figure A1-A80) 66
Figure 3.11. Vadose zone lag time vs depth to water table, mean hydraulic conductivity and soil moisture 67

List of Appendices

Annex 2.1. LAI values at study locations 81
Annex 3.1. The soil moisture at test locations 83
Annex 3.2. Depth to the water table in study locations 84
Annex 3.3. Travel time to groundwater table 85

List of parameters

Parameter	Description
(-)	Dimensionless units
α	Shape parameter in the van Genuchten water retention equation
c	Vertical soil moisture velocity
D_{rz}	Root zone depth
D_{wt}	Depth to water table
ET	Evapotranspiration
ET_a	Actual Evapotranspiration
ET_p	Biome-specific potential evapotranspiration
ET_0	Reference crop evapotranspiration
FC	Field capacity
PAW	Plant available soil moisture
K_c	Crop coefficient
K_s	Saturated hydraulic conductivity
LAI	Leaf area index
m	Shape parameter in the van Genuchten water retention equation (m=1-1/n)
n	Shape parameter in the van Genuchten water retention equation
std	Standard deviation
R_n	Net solar radiation
RI	Rainfall Interception
P	Precipitation
ρ	Correlation coefficient
$RMSE$	Root mean square error
θ	Volumetric water content
θ_r	Residual water content
θ_s	Saturated water content
T	Temperature
WP	Wilting point soil moisture
Z_{bot}	Depth to the water table or vadose zone thickness excluding root zone
τ	Vadose zone lag time
ψ	Pressure head

List of abbreviations

Parameter/abbreviation	Description
AI	Aridity index
ANN	Artificial Neural Network
FAO	Food and Agriculture Organization
GR	Groundwater Recharge
Har	Hargreaves
NAMEM	National Agency Meteorology and the Environmental Monitoring, Mongolia
NOAA	National Oceanic and Atmospheric Administration
PTF	Pedotransfer Function
Tho	Thornthwaite
SHC	Soil Hydraulic Characteristics

Acknowledgements

I would like to thank both the Fulbright scholarship for giving me the opportunity to study in the United States and the Daugherty Water for Food Institute for funding my research.

I would also like to express my deepest gratitude to my advisors Dr. Vitaly Zlotnik and Dr. Erin Haacker.

Dr. Vitaly Zlotnik guided me throughout my entire academic program. He has been the best mentor and advisor I could ever ask for. His help, guidance, and support were enormous, and I cannot even begin to list all that I learned from him. I will always be grateful to him, and I am confident that I will make good use of all that I learned from him in these last two years.

I feel very fortunate to have Dr. Erin Haacker, also, as my advisor. She truly cares about her students, and she sets an excellent example for them. Our weekly meetings have been a great help, as I could always ask questions and receive immediate assistance for my research. She is the most optimistic and talented woman I know, and she motivates me to work harder on my research.

I would also like to thank the rest of my dissertation committee: Dr. Andy Suyker, who taught me the basis of micrometeorology, evapotranspiration concepts, and very much needed guidance to the thesis.

I am also indebted to Dr. Paolo Nasta, who contributed to this research by giving valuable input and teaching me a lot through his great research experience.

Earnest thanks are due to Earth and Atmospheric Sciences department at UNL and its' very friendly and supportive staff.

I am also grateful to all my colleagues, friends, family, and everyone that helped me along the way and made it possible to be where I am today.

CHAPTER 1. INTRODUCTION

Land and water resources management in Mongolia relies on the knowledge of groundwater recharge (*GR*) replenishing aquifers that represent a vital water resource under an arid continental climate. However, in vast territories such as Mongolia, direct measurements of *GR* are unfeasible because they mandate excessive costs stemming from time-consuming and labor-demanding efforts. Alternative approaches to direct measurements are hydrological models simulating water balance within the groundwater-soil-plant-atmosphere continuum (Ma et al., 2003). The main advantage of using numerical models for Mongolia stems from the fact that the user needs "limited" data such as the monitoring of precipitation (*P*) and information to estimate evapotranspiration (ET). Like direct measurements of *GR*, direct measurements of *ET* (*i.e.*, eddy covariance technique, lysimeters, Bowen ratio energy balance, *etc*.) are logistically problematic, involve high investment/maintenance and are therefore completely unpractical for large-scale applications. However, limited data may be used to calculate the crop potential evapotranspiration (ET_0) and subsequent estimates of ET required for *GR* modeling. We recall that the vegetative-atmospheric evaporation/transpiration potential is expressed by the reference crop evapotranspiration (ET_0), representing the evapotranspiration flux from a standard, vegetated (*i.e.*, crop) surface in a well-watered field. The hypothetical reference crop is defined as having a height of 0.12 m, a surface resistance of 70 s m^{-1}, and an albedo of 0.23 (Allen et al., 1998). Due to a scarcity of data required to calculate this reference evapotranspiration, we opt to employ basic weather data recorded by relatively low-cost sensors installed in spatially distributed weather stations to estimate ET_0. Xiang et al. (2020) suggest it may be inappropriate to take natural vegetation as a

reference crop. As Mongolia is covered mainly by steppe grasslands under arid conditions, it is therefore necessary to convert ET_0 which is referenced to crops, into biome-specific potential evapotranspiration (ET_p) under optimal conditions. This ET_p represents the atmospheric evaporation demand, namely the amount of water that can be transferred to the air from land or water. Allen et al. (1998) discourage use of "potential evapotranspiration" term, but it's usage is still common in hydrologic applications, e.g., when there is a need to prepare ET_p for hydrological models. There are some usages of crop potential evapotranspiration term, but the biome specific potential evapotranspiration term was used in order to avoid confusion with agricultural crops. The developed K_c values will be used to convert reference crop evapotranspiration to specific biome in the region. Figure 1.1 portrays the selection of ET_0 method by testing proposed methods in 10 weather stations in Mongolia and the optimal steps to calculate *GR* with a hydrological model with using calculated ET_p and other required inputs in all 41 study locations.

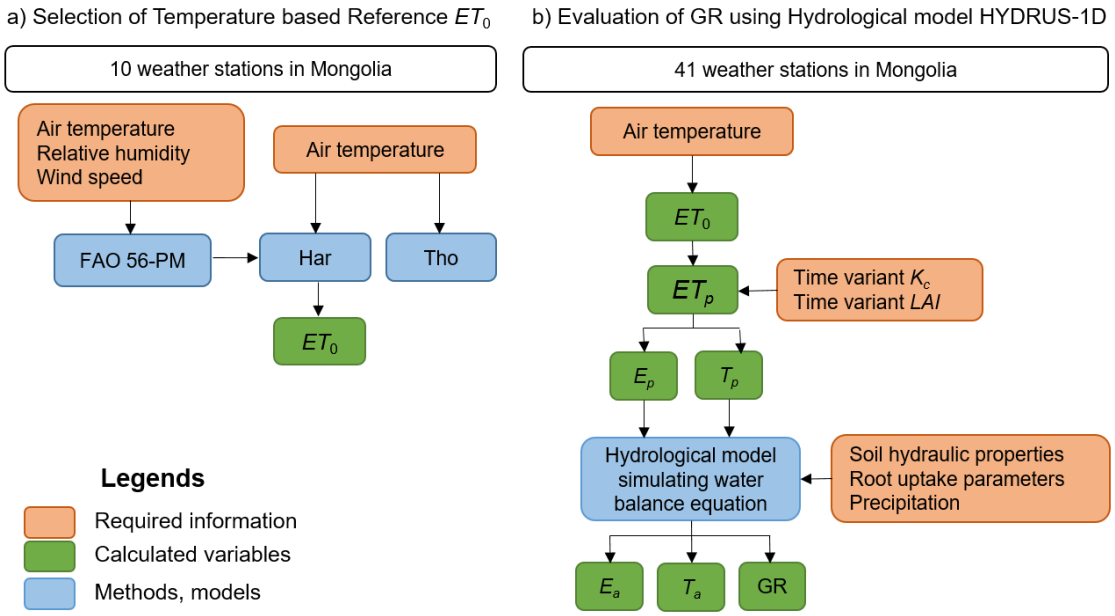

Figure 1.1. Schematic overview of the two steps to model ground water recharge (*GR*) involving a) estimation of reference evapotranspiration (ET_0) from basic weather data obtained employing three different estimates (FAO56-PM, HAR, and Tho) and (b) modeling process that starts with obtaining potential evapotranspiration (ET_p) and crop coefficient (K_c) and leaf area index (*LAI*) as the inputs to of a hydrological model that generates values of ground water recharge (*GR*).

The Chapter 2 will compare three ET_0 methods and seek the most suitable that utilizes simple, reliable, and easily retrievable basic weather information in Mongolia. Then the ET_p will be obtained by coupling selected ET_0 method with a term referred to as the crop coefficient (K_c) in 41 study locations. The effect of both crop transpiration and soil evaporation are integrated into a single crop coefficient (Allen et al., 1998). The K_c coefficient incorporates plant physiology and soil moisture deficit. However, for natural vegetation conditions, it is hard to fully specify the vegetation stress conditions and integrate them into the one K_c coefficient. The developed K_c depends on physiology but does not consider the soil moisture stress condition due to uncertainties related to the field condition while soil moisture deficit will be evaluated in HYDRUS-1D.

The Chapter 3 proceeds by using ET_p results for a soil-water balance model, focusing on *GR* in 41 study locations in Mongolia characterized by different environmental and climatic conditions. A reliable prediction of ET_p is fundamental in numerical models for obtaining the *GR* and actual evapotranspiration (ET_a). The obtained ET_p from developed K_c - s will be used to feed HYDRUS-1D, and the model will produce ET_a that represents a reduction of ET_p induced by water stress by evaluating the soil water condition in study locations. We assume that *GR* is equal to water drainage simulated at the end of the modeling depth in HYDRUS-1D.

Study locations

Mongolia is a landlocked country in north-central Asia, adjacent to China to the south and Russia to the north. Mongolia lies on a high plateau surrounded by mountain

ridges, in the transition zone between the Siberian taiga and the dry steppes and semi-deserts of central Asia (Yu et al., 2016). The country has a distinctly dry subarctic continental climate, with long cold winters and short hot summers. The mean annual precipitation (*P*) in Mongolia is about 200 mm, ranging from less than 50 mm in the Gobi Desert region to over 500 mm in the mountainous regions in the north. Maximum seasonal *P* occurs in summer (Yu et al., 2016). The 80% of Mongolia territory is comprised of pasture land, 10% forest, 1% farmland, and 9% other types of land. Steppe vegetation is the most common in Mongolia and occupies 1.03 million km^2, or 66% of the total territory (Indree, 2014). It lies mainly in the central part of the country, the transitional zone bordering the Gobi deserts to the south and mountain taiga forests to the north. The steppe ecosystems are associated with the semi-arid and arid continental temperate climates of the region and are ecologically fragile and sensitive to climate change and anthropogenic disturbances (Li et al., 2007). The perennial plants (50-90%) dominate the Mongolian steppe. The highest percentage of perennial plants occurs in the high-cold steppe, decreases eventually, and desert steppe has the least percentage (Indree, 2014). In contrast, the percentage of shrub, dwarf shrub, biennials, and annuals are the least in the high-cold steppe; it gradually increases and occupies half of the flora in the desert steppe (Indree, 2014). The average elevation of the country is about 1500 m and decreases gradually from the west to the east. Nearly half of the Mongolian territory consists of the mountains. These mountains are divided into Cool and Dry types according to their formation of vertical vegetation range. Khentii, Khuvsgul, northwestern Mongolian Altai, Northern Khangai, and Khyangan mountains refer to cool type and compose steppe vegetation of lower range. Southern Altai, Gobi Altai, Gobi,

and Zuungar mountains refer to dry type, and this type's specifics are that low range has desert vegetation and upper range has high-cold steppe (Indree, 2014).

We identified a total of 41 locations in Mongolia with weather data availability (Figure 1.2). We specify that ten weather stations (blue triangles in Fig. 2) provide a complete set of weather data while the remaining 31 stations provide only temperature (*T*) and *P* data. The study locations were chosen considering the density, physical geography, latitude, land use, climate class, and data availability.

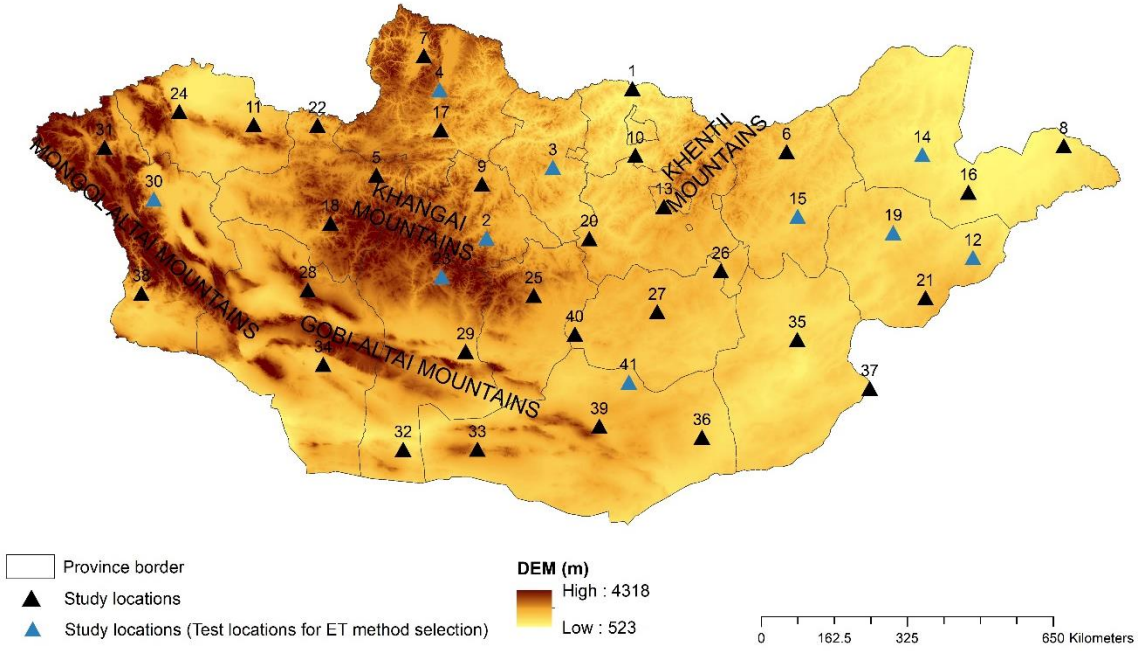

Figure 1.2. Locations of 41 weather stations (represented by the triangle symbol) on DEM (Digital Elevation Model) map retrieved from the Shuttle Radar Topography Mission (SRTM) in Mongolia (Earth Resources Observation And Science center, 2017). The ten blue triangles indicate the weather stations with a complete set of meteorological data used to compare FAO56-PM with temperature-based equations.

The study locations' IDs are shown in the map are used for presenting the results below. Complete data set belonging to the ten weather stations will be exploited for estimating ET_0 with FAO-56 PM equation and temperature-based equations (Chapter 2.).

CHAPTER 2. SELECTION OF EVAPOTRANSPIRATION METHOD

Introduction

First, we define evapotranspiration (ET) being the combination of two processes, namely soil surface evaporation (E) and crop transpiration (T). According to Allen et al. (1998), evaporation is the process whereby liquid water is converted to water vapour (vaporization) and removed from the evaporating soil surface (vapour removal). Transpiration consists of the vaporization of liquid water in plant tissues and the vapour transfer through plant stomata to the atmosphere. Stomata are small openings or pores on the plant leaf through which gases and water vapour pass. Together with some nutrients, the water is taken up by the roots and transported through the plant. The vaporization occurs within the leaf, namely in the intercellular spaces and sub-stomatal cavities, and the stomatal aperture controls the vapour exchange with the atmosphere. Nearly all water taken up is lost by transpiration, and only a tiny fraction is used within the plant (Allen et al., 1998).

The first step is to determine the optimal method to estimate ET_0 (reference crop evapotranspiration) in Mongolia. Two studies have been conducted with lysimeters (Table 1.1). First, according to Zhang et al. (2005), during the observation period, ET_a totaled 301.6 mm, and P totaled 319.5 mm, of which ET_a accounts for 94% of total P per year. While according to Li et al. (2007), cumulative ET_a during the study period estimated directly by the EC method was 163 mm, which was 66% of the P (248 mm) received at the site during the same period). Li et al. (2007) implies that the annual ET_a rate would have been accounted for 82–97% of the yearly precipitation rate, if significant

constraints such as canopy development and soil moisture conditions were taken into account more precisely.

Table 1.1. Previous ET studies in Mongolia

Study	Location	ET estimation method
(Zhang et al., 2005)	Nalaikh, Mongolia	Lysimeter
(Li et al., 2007)	Kherlenbayan-Ulaan (KBU), Khentii province, Mongolia	Lysimeter
(Nandintsetseg and Shinoda, 2011)	26 stations throughout the country	Thornthwaite formula (Thornthwaite, 1948)
(Batkhishig et al., 2013)	Meteorological stations with available data	Blaney, Criddle and Ivanov formula (Blaney and Criddle, 1962); Doorenbos and Pruitt (Doorenbos and Pruitt, 1977)
(Yu et al., 2016)	16 stations throughout the country	Penman-Monteith method

Meanwhile, studies by Nandintsetseg and Shinoda (2011), Yu et al. (2016), Batkhishig et al. (2013) have calculated ET in higher numbers of study locations. Nandintsetseg and Shinoda (2011) assumed the *GR* is negligible for the calculations, which can be a reasonable assumption for simplifying the water balance to estimate the soil moisture. However, even the small amount of *GR* can be huge input to the aquifer over a large area, and in order to assess sustainable water resources management, we need to quantify the *GR* correctly and understand its characteristics.

As seen from the previous studies, obtaining a reliable ET_p estimation can be problematic in Mongolia, and it depends on ET_0 and K_c values. The Penman-Monteith equation based on the Food and Agriculture Organization (FAO) guidelines (FAO-56 PM) is internationally recognized as the standard method for computing ET_0 (Allen et al., 1998; Yu et al., 2016). The equation is considered the most reliable method because it is based on the energy balance equation incorporating physiological and aerodynamic parameters without requiring any local calibration under all types of climatic conditions

(Allen et al., 1998). However, the FAO-56 PM method entails the availability of a complete set of weather data, including wind speed, air temperature, air relative humidity. These variables are often unavailable in data-limited countries where various meteorological parameters are hard to obtain or are available only in the form of useless short-time series. Challenges still exist nowadays, with some countries not having uniform distribution of full-suite weather sites, or lack of public access to the data, by hindering large-scale and long-term agro-hydrological studies. Nevertheless, long-term air temperature data are primarily available in spatially-dense weather networks across Mongolia.

Therefore we used two well-known limited-data requirement equations to predict ET_0, namely Hargreaves (hereafter referred to as Har; Hargreaves and Samani, 1985) and Thornthwaite (hereafter referred to as Tho; Mintz and Walker, 1993; Thornthwaite, 1948). First, we evaluate the prediction performance of Har and Tho equations by comparing these two methods with the FAO-56 PM equation by using a complete meteorological dataset that was available for ten weather stations. Second, the objectives of the study are twofold: *i*) to select a suitable temperature method, alternative to FAO-56 PM, to estimate ET_0; *ii*) to use a "dynamic" method for estimating a time-variant crop coefficient, K_c to convert ET_0 into ET_p.

In this study, the time-variant crop coefficient, K_c, depends on either radiation (Gobi Desert) or *LAI* (steppe zone) in Mongolia. Currently, the time-variant K_c – values are unavailable in Mongolia, and finding any reliable estimate of K_c can become the basis for further studies and potential improvements to predict ET_p. The proposed methodology

in this study can be used throughout the country to get reliable ET_p results with easily accessible parameters.

Methods

Determining the duration of the time series for simulation ET parameters

The monthly *P* and *T* at province centers (20 locations throughout the country) have been analyzed to choose the most representative years and characterize the climate in Mongolia. Figure 1.1. shows *T* and *P* data from the weather stations in province centers that have been averaged between all stations from 2005 to 2019. Average *T* ranges from around -0.1 °C to 2.6 °C while average *P* ranges from about 130 mm to 260 mm.

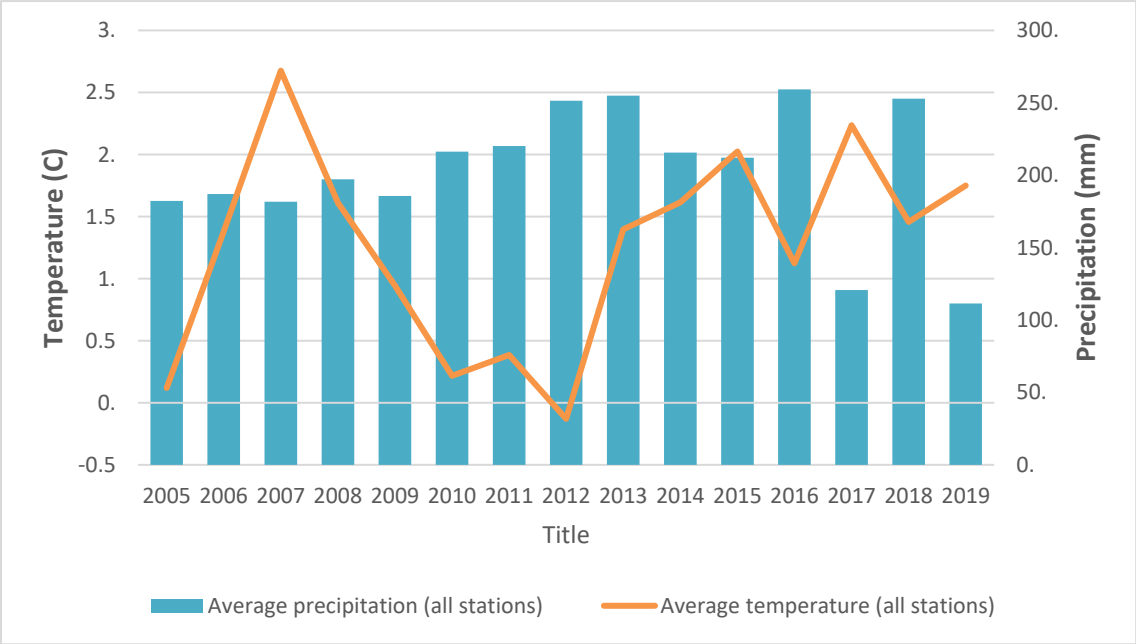

Figure 1.1. The mean precipitation and temperature /average of all available stations data/

The annual *T* and *P* data from 2005-2019 has been analyzed in order to choose the shorter period, which can represent this whole time series. According to the results, the 2007-2011 cycle has the closest *T* and *P* mean results with the entire series. The mean *P* of 2007-2011 in all stations lies within one *std* range from the entire series, while the mean *T* of 2007-2011 in 20 stations from a total of 21 stations lies within one *std* range

from the entire series. The 2007-2011 period was the most representable of the entire series and therefore chosen for the study.

Approaches to ET estimation

In this study, we considered three methods to estimate ET_0:

- Penman-Monteith (denoted as FAO-56 PM)
- Hargreaves (denoted as Har)
- Thornthwaite (denoted as Tho)

The development of ET_0, although initially confused with ET_p, was formally defined as a standard method by Allen et al. (1998). Due to vagueness in its definition, ET_p was not always applied properly (Xiang et al., 2020). The FAO-56 PM is recommended as the sole standard method to calculate ET_0. Given the complete meteorological data availability over ten weather stations, we compare the FAO-56 PM equation with evapotranspiration models of Har (Hargreaves and Samani, 1985) and Tho (Thornthwaite, 1948; Mintz and Walker, 1993). After selecting the best temperature model, ET_0 will be calculated in all 41 study locations with daily temperature data. The analytical equations of these methods are reported in Table 1.2, and we briefly report necessary input data for each equation.

Table 1.2. FAO-56 PM, Har and Tho equations with required input data

Methods	Minimum meteorological data requirements						Equations
	Aver T°	Max T°	Min T°	Rel. humi-dity	Wind speed	R_a or R_n	
FAO-56 PM	+	+	+	+	+	+	$ET_0 = \frac{0.408\Delta(R_n - G) + \gamma\frac{900}{T+273}u_2(e_s - e_a)}{\Delta + \gamma(1 + 0.34u_2)}$

Hargreaves	+	+	+			+	$ET_0 = 0.0023(T_m + 17.8)(T_{max} - T_{min})^{0.5}(0.408R_a)$
Thornthwaite modified	+						$ET_0 = \begin{cases} 0, & T < 0^\circ \\ 0.553\left(\frac{10T}{I}\right)^{\alpha}, & 0 \le T \le 26.5^\circ \\ (-13.86 + 1.075T - 0.0144T^2)\frac{h}{12}, & T \ge 26.5^\circ \end{cases}$ $I = \sum_1^{12}\left(\frac{T_m}{5}\right)^{1.514}$ $\alpha = (6.75 \times 10^{-7} I^3) - (7.71 \times 10^{-5} I^2) + (1.79 \times 10^{-2} \mathrm{I}) + 0.492$

In the FAO-56 PM equation, R_n is net radiation at crop surface (MJ m^{-2} d^{-1}), G is the soil heat flux density (MJ m^{-2} d^{-1}), T is air temperature (°C), u_2 is the wind speed at 2 m height above ground (m s^{-1}), e_s and e_a are saturated and actual vapour pressures (kPa), Δ is the slope of the vapour pressure curve (kPa $°C^{-1}$) and γ is the psychometric constant (kPa $°C^{-1}$). Net radiation is usually indirectly measured by a pyranometer. We remind that if weather stations lack pyranometers, R_n can be estimated from the actual daily duration of bright sunshine (hours per day). The term G is computed as a fraction of R_n as suggested by Allen et al. (1998) for the reference crop. In the Har equation, R_a is the extraterrestrial radiation expressed in mm d^{-1}, T_m (°C), T_{min} (°C), and T_{max} (°C) represent mean, minimum and maximum temperature, respectively. In the Tho equation, a value I represents the annual heat index, T_m represents i-th month mean air temperature (°C), and h depicts hours of sunlight (hours).

Evaluation criteria

To measure the predictive capability of the tested Har and Tho methods, we selected two statistical performance indicators: the Root Mean Square Error (*RMSE*),

which combines both bias and lack of precision, and the coefficient of determination (R^2), which measures how well the data pairs fit to a line:

$$RMSE = \sqrt{\frac{1}{n}\sum_{i=1}^{n}(\hat{o}_i - \hat{e}_i)^2} \quad (1)$$

$$R^2 = \frac{\sum_{i=1}^{n}(\hat{o}_i - \hat{e}_i)^2}{\sum_{i=1}^{n}(\hat{o}_i - \tilde{o})^2} \quad (2)$$

where $\hat{o}_i$ is the observed value (reference value, FAO-56 PM ET_0), $\tilde{o}$ is the mean of observed values, and $\hat{e}_i$ indicates estimated values of ET_0 (ET_0-Har and ET_0-Tho). Subscript *i* is the counter for time values (in day units), and *n* is the total number of days. Daily values of ET_0 will also be aggregated at monthly and annual sums; therefore, *RMSE* units are also expressed as mm month^{-1} and mm year^{-1}, respectively. For an optimal prediction, values should be as low as possible for *RMSE* and as close as possible to 1 for R^2.

Crop coefficients, K_c

The K_c is required to convert ET_0 into ET_p. Many studies have been undertaken for finding ET_0 and K_c, but they were mainly focused on croplands (Jia et al., 2009; Kjaersgaard et al., 2008; Suleiman et al., 2007; Suyker & Verma, 2009). Very few studies have been conducted in semi-arid natural environments (Zhang et al., 2012). Crop-specific K_c values in Mongolia are currently unavailable in pristine or anthropogenically affected areas. The K_c coefficient incorporates crop characteristics and averaged effects of evaporation from the soil (Allen et al., 1998). But for natural vegetation conditions, it is hard to fully specify the vegetation stress conditions and integrate them into the one K_c coefficient. The developed K_c depends on physiology but does not consider the soil

moisture stress condition due to uncertainties related to the field condition in study locations. The soil water condition will be evaluated in HYDRUS-1D for obtaining ET_a from ET_p.

The study locations spread over various natural zones which are representative of 83% of Mongolia. Nevertheless, the natural zones can be further grouped into land cover zones of the Gobi Desert and the steppe (Table 1.3). Previous studies have indicated that the K_c values vary significantly during the growing season; therefore, it is impossible to assume K_c as constant over time. Thus, the potential time-variable methods were attempted to be implemented in the study across the two land cover zones (Gobi Desert and the steppe).

Table 1.3. Categorization of natural zones

ID	Stations	Natural zone	ID	Stations	Natural zone
1	Sukhbaatar	steppe	22	Baynuul	steppe
2	Tseterleg	steppe	23	Galuut	steppe
3	Bulgan Mg	steppe	24	Ulaangom	steppe
4	Khatgal	steppe	25	Arvaikheer	steppe
5	Tosontsengel	steppe	26	Choir	steppe
6	Binder	steppe	27	Mandalgobi	steppe
7	Rinchinlhumbe	steppe	28	Altai	steppe
8	Khalkh gol	steppe	29	Khoriult	steppe
9	Erdenemandal	steppe	30	Khovd	Gobi Desert
10	Baruunkharaa	steppe	31	Ulgii	Gobi Desert
11	Baruunturuun	steppe	32	Ekhiingol	Gobi Desert
12	Erdenetsagaan	steppe	33	Gurvantes	Gobi Desert
13	Chingis khaan (UB)	steppe	34	Tooroi	Gobi Desert
14	Choibalsan	steppe	35	Sainshand	Gobi Desert
15	Undurkhaan	steppe	36	Khanbogd	Gobi Desert
16	Matad	steppe	37	Zamiin Uud	Gobi Desert
17	Murun	steppe	38	Baitag	Gobi Desert
18	Uliastai	steppe	39	Dalanzadgad	Gobi Desert
19	Baruun-Urt	steppe	40	Saikhan-Ovoo	Gobi Desert
20	Erdenesant	steppe	41	Tsogt-Ovoo	Gobi Desert
21	Dariganga	steppe			

This study attempts to propose a dynamic (time-variant) K_c using easily-retrievable data such as solar radiation or *LAI*. According to Xia et al. (2014), the

normalized difference vegetation index (NDVI) showed strong positive correlations with evapotranspiration over the majority of grassland areas except for the region near the Gobi Desert (Lamchin et al., 2015). This indicates the regular K_c evaluation might not be suitable in the Gobi Desert area, and some research in Inner Mongolia (China) supports this assumption (Zhang et al., 2012). Thus, the area-specific K_c should be used for the Gobi Desert area in Mongolia. According to Yang and Zhou (2011), by indicating the day of the year (DOY), daily K_c values in the growing season ranged from 0.02 to 0.50 with an average value of 0.17 in a temperate desert in Inner Mongolia. Therefore, according to Zhang et al. (2012), K_c during the study period averaged from 0.15 to 0.17 in Inner Mongolia. Both studies were performed in the Gobi Desert (China) and are taken as representative of the Gobi Desert in Mongolia. Since both studies match well, the regression equation from Yang and Zhou (2011) is implemented in Gobi Desert study locations in order to estimate temporal variations of K_c:

$$K_c = 0.02 * R_n \quad (3)$$

where K_c is the crop coefficient, and R_n is net radiation.

In the steppe zone in Mongolia, similar studies are scarce, and there are no readily available crop coefficients developed for natural vegetation from FAO-56 documents (Allen et al., 1998). The guideline by Allen et al. (1998) for developing K_c for (non-crop) grassland in arid climates require parameters such as vegetation height, air relative humidity, and wind speed, and due to the data deficiency, the method is not used for our study. Instead, the method which can be developed with easily available data has been explored. According to Sumner and Jacobs (2005), the crop coefficients in a non-irrigated

pasture site in Florida, USA, ranged from 0.47 to 0.92 and could be calculated from a linear function of leaf area index (*LAI*):

$$K_c = \alpha LAI + b \quad (4)$$

where empirical parameters are assumed as a=0.330 and b=0.451.

Format of equation 4 is useful as an approximation for K_c during the mid-season stage for crops that almost shade the soil under pristine conditions. The natural vegetation condition in study locations has various constraints to the vegetation growth and does not have its optimal vegetation cover. In order to use equation 4, we proposed to reduce the K_c by introducing an adjustment. There is no guidance for specific adjustment in Mongolia, but the following general equation was proposed by Allen et al. (1998) for sparse vegetation:

$$K_{c\ adj} = K_c - A_{cm} \quad (5)$$

where $K_{c\ adj}$ is the adjustment parameter, and A_{cm} is another empirical coefficient given by the equation:

$$A_{cm} = 1 - \left[\frac{LAI}{LAI_{dense}}\right]^{0.5} \quad (6)$$

where LAI_{dense} is the *LAI* expected for the same crop under normal, standard crop management practices. The LAI_{dense} can be predicted from the ground cover ratio at the sites and will differ among locations.

The same function could not be applied in all study locations throughout the steppe due to contrasting vegetation characteristics. After multiple attempts, the LAI_{dense} values in the steppe zone in study locations with higher-than-average *LAI* values ($LAI > 0.6$) and locations with lower-than-average values ($LAI < 0.6$) were calculated using different equations:

$$LAI_{dense} = \begin{cases} \frac{0.95 - 0.2}{0.6 - 0} LAI + 0.2, & LAI < 0.6 \\ \frac{3.03 - 0.95}{2.53 - 0.6}(LAI - 0.6) + 0.95, & LAI > 0.6 \end{cases} \quad (7)$$

Figure 1.2 shows A_{cm} and LAI_{dense} as a function of LAI.

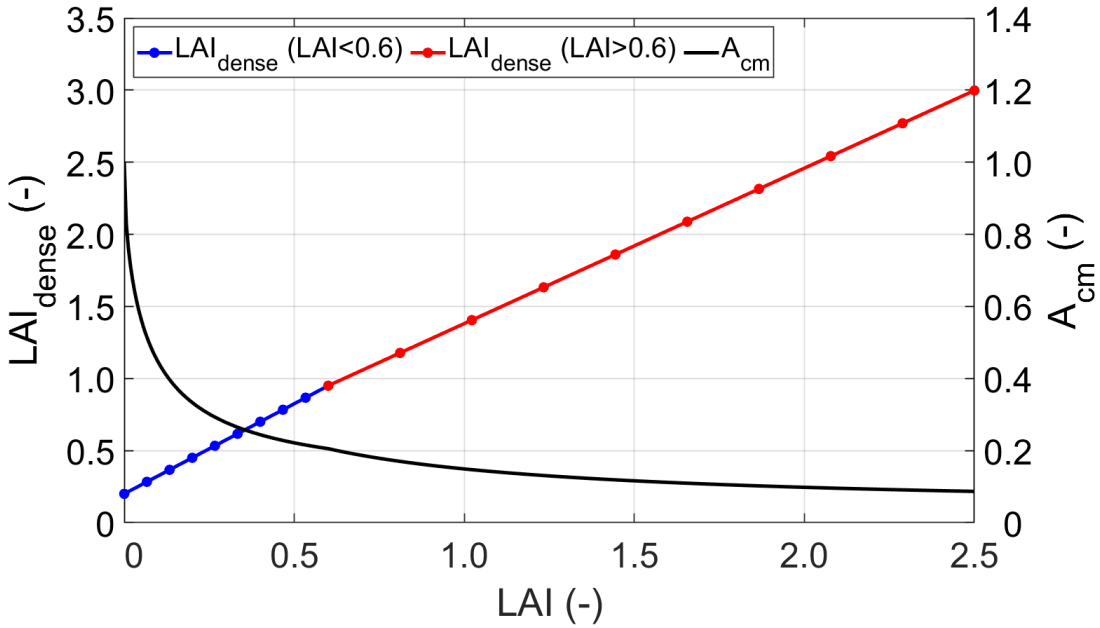

Figure 1.2. LAI_{dense} and A_{cm} values depending on LAI.

In the steppe zone, as a result of experimentation, LAI_{dense} can not be calculated with the same function in all locations with different vegetation cover. LAI_{dense} is calculated from LAI, and the 0.6 point in LAI is proposed to be the transitional point (Figure 1.2). With LAI_{dense} results, the A_{cm} and $K_{c\ adj}$ can be calculated, and therefore ET_p values can be obtained using these $K_{c\ adj}$ results in study locations of the steppe zone.

The growing season has been identified as starting 7 days before last temperature -4°C in spring until 7 days after first temperature -4°C in fall in all study locations, assuming as grass pasture from FAO-56 document (Allen et al., 1998). The K_c in the non-growing season is considered as 0.05 in all study locations by the guidance of Allen et al. (1998) for calculating evaporation in non-growing seasons.

The ET_p will be calculated from ET_0 and developed K_c-s. This ET_p represents the atmospheric evaporation demand, namely the amount of water that can be transferred to the air from land or water. And the developed K_c-s convert reference crop evapotranspiration to a specific biome in the region. There are some usages of crop potential evapotranspiration term (Adane et al., 2019; Lewis & Allen, 2017), but in order to avoid confusion with agricultural crops, the biome-specific potential evapotranspiration term has used. The ET_a will be obtained by evaluating the soil water condition and will be reduced from ET_p by water stress in study locations by HYDRUS-1D.

Evaporation and Transpiration

Vegetation plays a vital role in partitioning solar energy into evaporation from the land surface and transpiration through the vegetation. A "Beer's law" approach partitions the solar radiation component of the energy budget into potential E_p and T_p via interception by the canopy (Ritchie, 1972) using the leaf are index (*LAI*):

$$E_p = ET_p e^{-k*LAI} = ET_p(1 - SCF) = ET_p e^{-0.463LAI} \quad (8)$$

$$T_p = ET_p(1 - e^{-k*LAI}) = ET_p SCF = ET_p - E_p \quad (9)$$

where ET_p – potential evapotranspiration,
E_p – potential evaporation,
T_p – potential transpiration,
LAI – the leaf area index [-],
SCF – soil cover fraction [-],
k is a constant (0.463) governing the radiation extinction by the canopy [-]

Previous studies (Adane et al., 2018; Ritchie, 1972) have typically used a coefficient k = 0.463 for different types of vegetation, and this coefficient was used in our study.

The FAO Aridity Index, *AI*

The *AI* (Aridity index) is computed as the average of the ratio between annual total *P* and ET_p (Spinoni et al., 2015) over a set time period (5 years in our case):

$$AI = \frac{1}{5}\sum_{i=1}^{5}\frac{P_i}{ETp_i} \quad (10)$$

AI is computed as the average of the ratio between annual total precipitation (*P*) and potential evapotranspiration (ET_p), and *i* denotes the *i*-th year. The classification of *AI* by FAO is shown in Table 1.4.

Table 1.4. Macro-classes and classes of the FAO *AI*

Macro-class	Class	Value
Arid	Desert	AI≤0.03
	Hyper-Arid	0.03<AI≤0.05
	Arid	0.05<AI≤0.2
	Semi-Arid	0.2<AI≤0.5
Mid	Dry	0.5<AI≤0.65
	Sub-humid	0.65<AI≤0.75
Humid	Humid	AI>0.75
Cold	Cold	ET_P≤400 mm

The *AI* results can be a good illustration of classification of study locations for various analyses.

Data collection

In order to select the applicable method in Mongolia, the daily maximum, minimum, average temperature, relative humidity, and wind speed data were obtained from NAMEM (http://tsag-agaar.gov.mn) in ten test locations. The hours of sunlight data were obtained by WeatherOnline Ltd (2021) at the nearest available station from (https://www.weatheronline.co.uk/). The terms R_a and R_n were indirectly estimated from the guidelines on missing climatic data from the FAO-56 report (Allen et al., 1998). For the chosen method, Table 1.5 gives details on the data available for the 41 study locations.

Table 1.5. Data sources

Collected data/parameters	Unit	Location	Period of data availability	Source	References
Daily *P*	mm	Study locations are shown in Fig. 2.	2007-2011	NAMEM	(National Agency for Meteorology and Environmental Monitoring)
Daily max *T*, min *T*, average *T*	(C^o)	Study locations are shown in Fig. 2.	2001-2020	NOAA National Centers for Environmental Information	(Menne et al., 2012)
LAI	(-)	Locations are shown in Fig. 3.	1981-2015	ORNL DAAC	(Mao and Yan., 2019)

Temperature

T measurements were obtained from National Oceanic and Atmospheric Administration (NOAA) website (https://www.ncdc.noaa.gov/cdo-web/) (Menne et al., 2012), and the reliability of the data was tested in the following part. Remotely sensed and ground-based measured *T* data are strongly correlated (Figure 1.3).

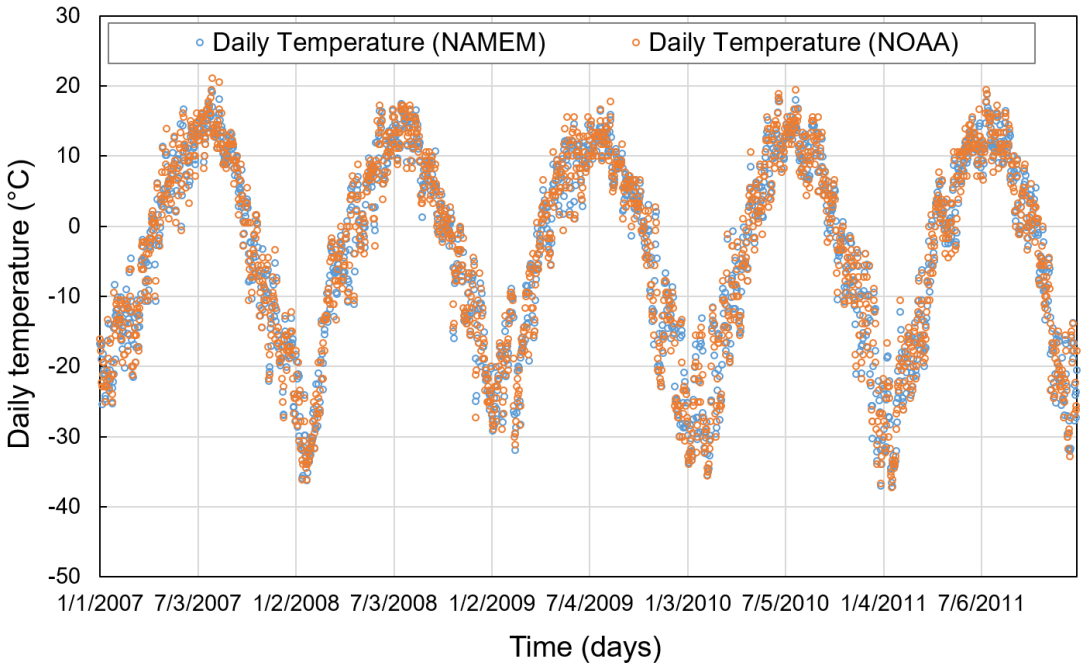

Figure 1.3. The comparison of daily temperature measurements in Khatgal

As seen from the figure, the remotely measured temperature data potentially can replace the ground measured temperature. Thus the T measurements from NOAA (Menne et al., 2012) are collected in 41 study locations.

Leaf Area Index, *LAI*

The region's climate is characterized by a long and cold winter and a short but warm summer (Romanova et al., 1983). The development of vegetation cover depends on the quantity plus the seasonal and geographical distribution of precipitation. The geobotanical diversity of Mongolia is extremely high. Mongolia extends over 1,200 km from the north to the south, and one can find a spectrum of the landscape as in the temperate belt of Eurasia, e.g., from typical forests to extra-arid deserts. The contrasts in these communities cause compression of vegetation zones, and very high gradient changes are characteristic of the vegetation cover. However, a wide spectrum of the zones and interzonal transitions exist. The dynamics of Mongolia's vegetation are

controlled by changes in climatic parameters (a decrease and long-term oscillations in precipitation), an intensification of natural destructive processes that are subject to the influence of economic activity, improper nature management practices, and numerous direct human-associated disturbances and changes in vegetation cover. The natural pasture land can be divided into 200 types of pasture, and 900 of the total 2,800 plant species that are documented in Mongolia are vascular plants and are used for livestock forage. Since Mongolia is located between the Siberian taiga in the north and the Gobi Desert in the south, the pasture vegetation decreases from north to south (Khishigsuren and Linden, 2012).

LAI was collected from literature and remotely sensed products. Since the *LAI* measurements are highly time-variable and differ a lot throughout the country, the spatial results from the remotely sensed products were much efficient. The *LAI* monthly mean values were obtained from the global monthly mean *LAI* climatology index, 1981-2005 (Mao and Yan., 2019). This dataset provides a global 0.25^{o} x 0.25^{o} gridded monthly mean *LAI* climatology as averaged over the period from August 1981 to August 2015. The data were derived from the Advanced Very High-Resolution Radiometer (AVHRR) Global Inventory Modeling and Mapping Studies (GIMMS), and the bi-weekly *LAI* values were averaged for every month. Then, the monthly long-term mean *LAI* (1981-2015) was calculated (Mao and Yan, 2019).

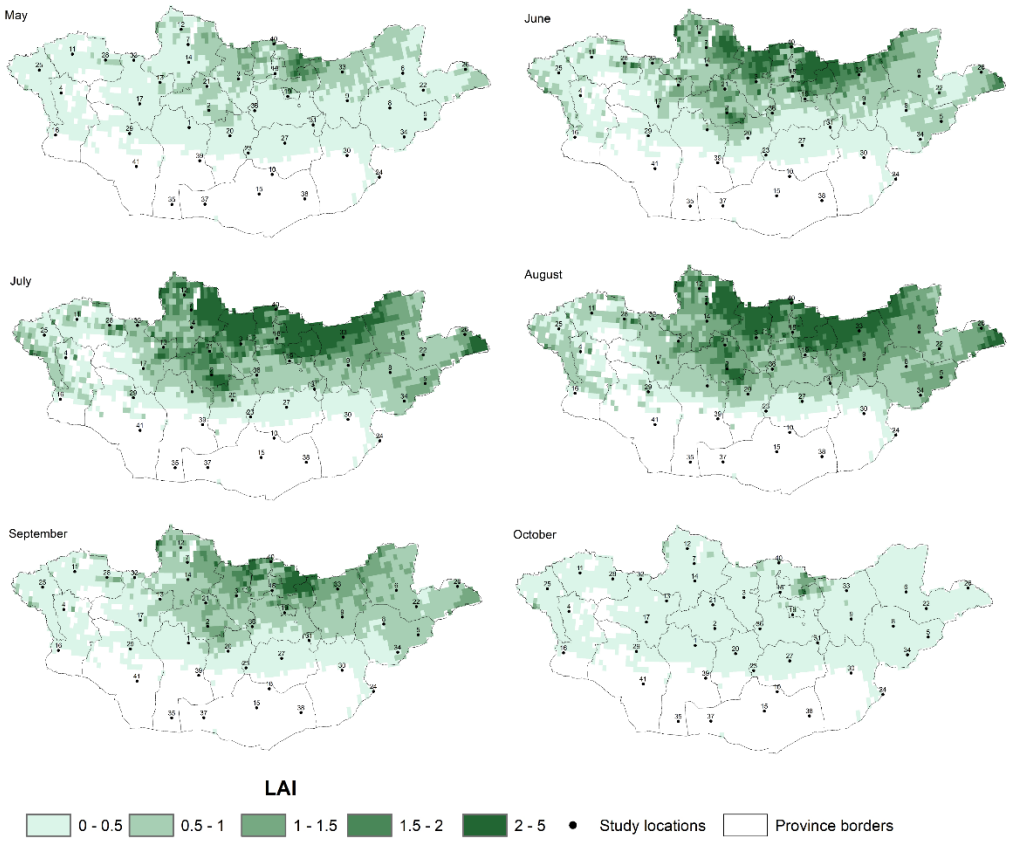

Figure 1.4. Map showing the monthly mean *LAI*s in the growing season, extracted from the dataset by (Mao & Yan., 2019).

Due to the low cover of vegetation and bushy vegetation, the *LAI* in the Gobi area from the maps was unknown. The *LAI* values from the closest locations are used to represent the *LAI* in Gobi Desert locations. The monthly *LAI* values at study locations are shown in Annex 2.1. The daily *LAI* has calculated from linear interpolation in 41 study locations. Then the extracted *LAI* values have used to partition the $ET_{p,}$ as shown in equations 8 and 9.

Results and discussion

The method selection for reference crop evapotranspiration, ET_0

In order to understand the relationship between meteorological variables and FAO-56 PM, ET_0 over the ten weather stations is expressed in terms of Pearson correlation coefficients presented in Table 1.6.

Table 1.6. Pearson correlation coefficients between FAO-56 PM ET_0 and meteorological variables over the ten weather stations in Mongolia

	Wind speed	Relative humidity	Air temperature	Net radiation	Sunshine hours
1.Galuut	0.51	-0.57	0.91	0.92	0.74
2.Tsetserleg	0.16	-0.23	0.91	0.91	0.84
3.Bulgan	0.30	-0.47	0.90	0.92	0.75
4.Khovd	0.58	-0.76	0.90	0.92	0.84
5.Erdenetsagaan	-0.02	-0.63	0.91	0.88	0.69
6.Choibalsan	0.04	-0.69	0.91	0.91	0.83
7.Khatgal	0.01	-0.28	0.90	0.92	0.85
8.Baruunurt	0.20	-0.72	0.91	0.90	0.71
9.Undurkhaan	0.20	-0.73	0.90	0.90	0.72
10.Tsogtovoo	0.21	-0.68	0.91	0.91	0.84

Note: the dark blue color indicates a high correlation coefficient (close to 1)

High positive correlation coefficients are observed between ET_0 and air temperature and net radiation, while negative correlation coefficients are reported when relating ET_0 with relative humidity. The results agree with the conclusion of Wang et al. (2007) that the net radiation and air temperature are the most important controlling factors on ET_0, which is evidence of the potential of temperature-based ET_0 models.

The accuracy of Har and Tho methods is assessed by computation of daily *RMSE* and R^2 values quantifying the relationship with FAO-56 PM (Figure 1.5).

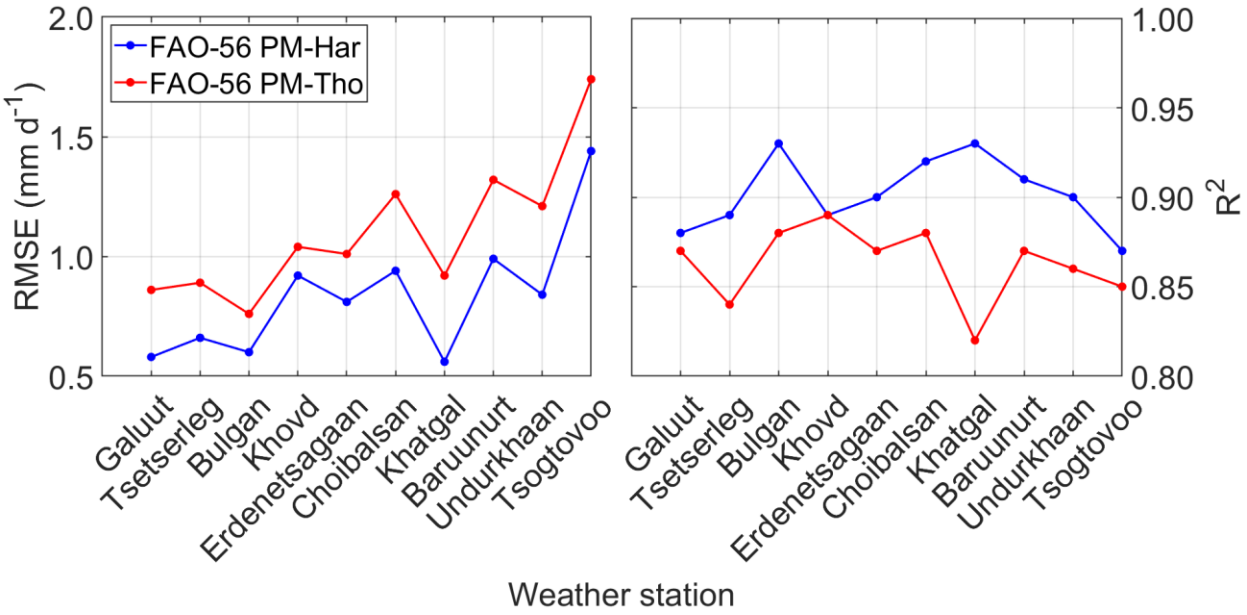

Figure 1.5. Model performance indicators comparing the FAO-56 PM with Har (blue line) and Tho (red line) to estimate daily values of ET_0: (a) *RMSE* (mm d^{-1}) values and (b) values of R^2 (-) for ten weather stations.

The comparison between Har and FAO-56 PM equations (blue line in Figure 1.5) leads to a minimum *RMSE* of 0.56 mm d^{-1} in Khatgal (R^2=0.93) and maximum *RMSE* of 1.44 mm d^{-1} in Tsogtovoo (R^2=0.87). The average *RMSE* is 0.83 mm d^{-1} and R^2=0.90. The comparison between Tho and FAO-56 PM equations (red line in Figure 1.5) leads to a minimum *RMSE* of 0.76 mm d^{-1} in Bulgan (R^2=0.88) and maximum *RMSE* of 1.74 mm d^{-1} in Tsogtovoo (R^2=0.85). The average *RMSE* is 1.10 mm d^{-1} and R^2=0.86. The Har ET_0 method shows lower *RMSE* and higher R^2 than those obtained from the Tho equation over the 10 test locations. The inaccuracy in a temperature-based model in estimating ET_0 is attributed to their inability to consider meteorological variables such as relative humidity, solar radiation, and vapor pressure deficit as diagnosed by high correlation coefficients listed in Table 5. Similar *RMSE* values between FAO-56 PM and uncalibrated Har equation are reported in southern Italy (Pelosi et al., 2016), in south-east Spain (Gomariz-Castillo et al., 2018), in the U.S. High Plains (Kukal et al., 2020),

northwest China (Celestin et al., 2020), while lower *RMSE* values are reported in arid and semi-arid areas in China (Gao et al., 2017).

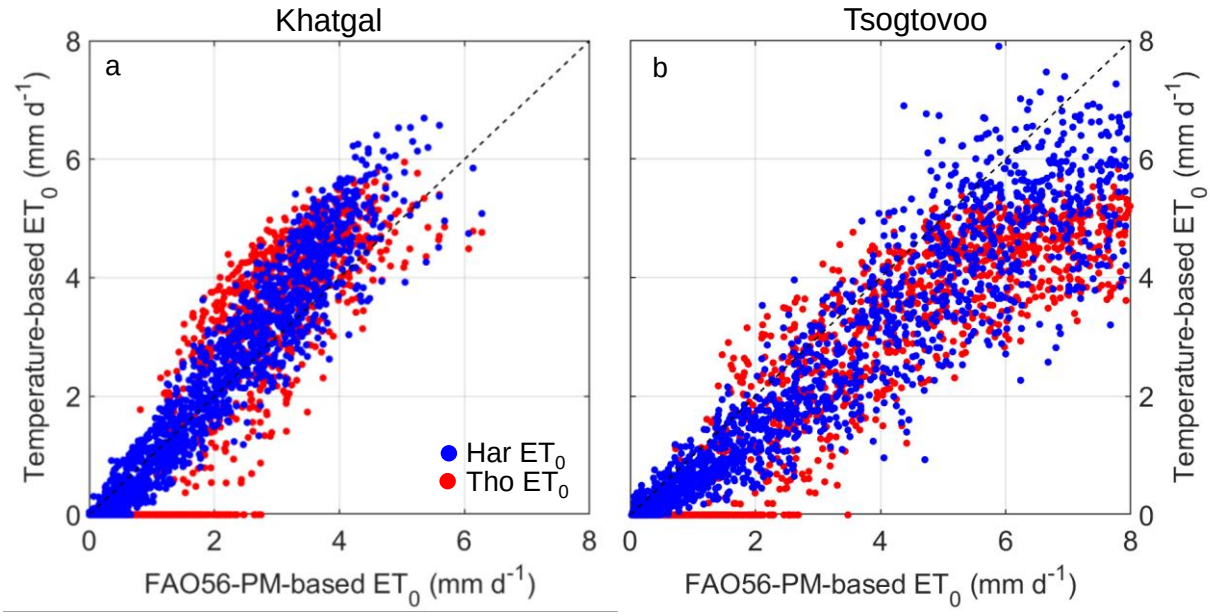

Figure 1.6. Comparison between FAO-56 PM-based and temperature-based equations (Har ET_0 values are represented by blue circles and Tho ET_0 values are depicted by red circles) for predicting daily values of ET_0 at (a) Khatgal weather station, and b) Tsogtovoo weather station.

Figure 1.6 shows a comparison between FAO-56 PM-based and temperature-based equations over Khatgal and Tsogtovoo weather stations, where we obtained the best and worst performance, respectively. A closer inspection of Figure 1.6 reveals several zero values of ET_0 predicted by the Tho equation that might suffer from underestimation if compared to the Har equation.

The annual average ET_0 sums by three methods are visualized in Figure 1.7. The FAO-56 PM-based predictions annual average ET_0 sums are in accordance with the estimates in Inner Mongolia (China) reported by Bian et al. (2020).

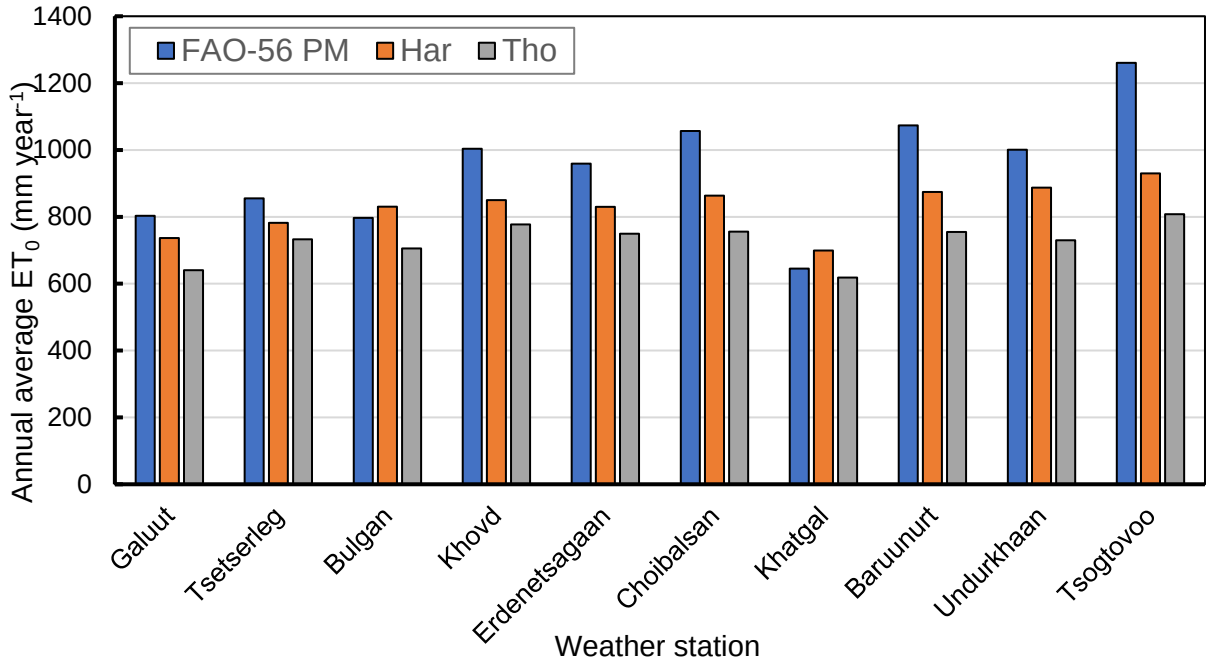

Figure 1.7. Annual average ET_0 calculated with FAO56-PM (blue bars), Har (orange bars), and Tho (gray bars) for ten weather stations in Mongolia.

Both Har-based and Tho-based models tend to underestimate FAO-56 PM-based average annual ET_0 in most weather stations. The underestimation is observed in other studies evaluating the Har model in arid and semi-arid conditions in several parts of the world (Amatya et al., 1995; Mohawesh and Talozi, 2012; Xu and Singh, 2002; Tabari and Talaee, 2011). As expected from previous outcomes, the annual average ET_0 sums based on the Har method are closer to FAO-56 PM in 9 out of 10 weather stations when compared to the Tho equation performance. The monthly cumulative FAO-56 PM ET_0 also better matches the result from the Har method. One of the drawbacks of the Tho method is that ET_0 cannot be used in winter months when the temperature drops below 0 °C. Therefore, according to the cumulative results, the Tho method systematically underestimates the ET_0. As seen from the statistical results and cumulative comparisons, the Har outperforms the Tho equation for estimating ET_0; thus Har ET_0 method is selected in the study.

Reference crop evapotranspiration results

Daily values of ET_0 were calculated by using the selected Har method over the 41 study locations between 2007 and 2011 that had the same mean and standard deviation as any other 5-year cycle. Annual sums of ET_0 are presented in Table 1.7.

Table 1.7. Annual sums of ET_0 over the 41 weather stations in Mongolia

№	Stations	Annual Har ET_0 (mm)					Average mean Har ET_0 (mm)	CV (%)
		2007	2008	2009	2010	2011		
1	Sukhbaatar	861	847	929	812	812	852	5.6
2	Tseterleg	845	819	801	763	769	799	4.3
3	Bulgan Mg	891	854	854	835	782	843	4.7
4	Khatgal	742	715	694	691	695	707	3.0
5	Tosontsengel	791	762	753	696	729	746	4.8
6	Binder	907	818	823	793	840	836	5.1
7	Rinchinlhumbe	723	686	663	666	687	685	3.5
8	Khalkh gol	910	872	834	863	839	863	3.5
9	Erdenemandal	871	836	810	793	789	820	4.2
10	Baruunkharaa	921	889	884	846	849	878	3.5
11	Baruunturuun	792	769	727	713	749	750	4.2
12	Erdenetsagaan	926	848	847	849	820	858	4.7
13	Chingis khaan (UB)	584	561	571	757	694	634	13.8
14	Choibalsan	952	881	876	860	880	890	4.0
15	Undurkhaan	987	914	883	874	894	910	5.0
16	Matad	976	882	882	877	854	894	5.3
17	Murun	865	834	814	777	798	817	4.1
18	Uliastai	842	818	790	755	772	795	4.4
19	Baruun-Urt	972	896	900	880	862	902	4.6
20	Erdenesant	881	843	804	772	750	810	6.5
21	Dariganga	835	841	819	864	866	845	2.4
22	Baynuul	819	770	741	714	735	756	5.4
23	Galuut	769	797	763	739	708	755	4.4
24	Ulaangom	863	846	798	790	819	823	3.8
25	Arvaikheer	830	808	825	780	776	804	3.1
26	Choir	954	893	898	857	839	888	5.0
27	MandalGobi	954	915	922	861	871	905	4.2
28	Altai	778	753	740	691	706	733	4.8
29	Khoriult	987	982	1001	955	952	975	2.2
30	Khovd	902	898	867	824	846	867	3.9
31	Ulgii	846	838	781	777	808	810	3.9
32	Ekhiingol	1121	1139	1159	1106	1118	1129	1.8
33	Gurvantes	886	891	921	869	871	888	2.4
34	Tooroi	1104	1130	1121	1039	1038	1086	4.1

35	Sainshand	1029	1000	1012	984	952	996	2.9
36	Khanbogd	1034	995	1029	971	983	1002	2.8
37	Zamiin Uud	1033	1010	1041	1002	1010	1019	1.7
38	Baitag	1000	1006	957	886	964	962	5.0
39	Dalanzadgad	985	985	1012	964	960	981	2.1
40	Saikhan-Ovoo	981	957	1003	946	926	963	3.1
41	Tsogt-Ovoo	1015	985	1012	955	936	981	3.5
Spatial-average ET_0		902	873	867	840	843		

According to Table 1.7, the ET_0 annual sums broadly vary in space with low temporal variability in each station through 5 years. The coefficient of variation (*CV*) is lower than 10% in 40 out of 41 stations. If we consider the spatial-average ET_0 in each year, 2007 and 2011 have the highest and lowest values, respectively.

The Har ET_0 results are close to the previous studies carried out in Mongolia (Li et al., 2007; Zorigt et al., 2012; Yu et al., 2016). However, to our knowledge, there is a lack of studies on ET_0 in the period 2007-2011. A global map of monthly reference evapotranspiration obtained from FAO (2009) was chosen for comparison among the available remote sensing products. The map was produced by using the FAO-56 PM method with a spatial resolution of 10 arc minutes. The monthly map was developed from the various meteorological datasets for the period 1961-1990; thus, it is assumed to be representative of mean monthly ET_0 results. To be consistent with our study, the mean annual ET_0 (Figure 1.8) map is obtained from the monthly ET_0 maps.

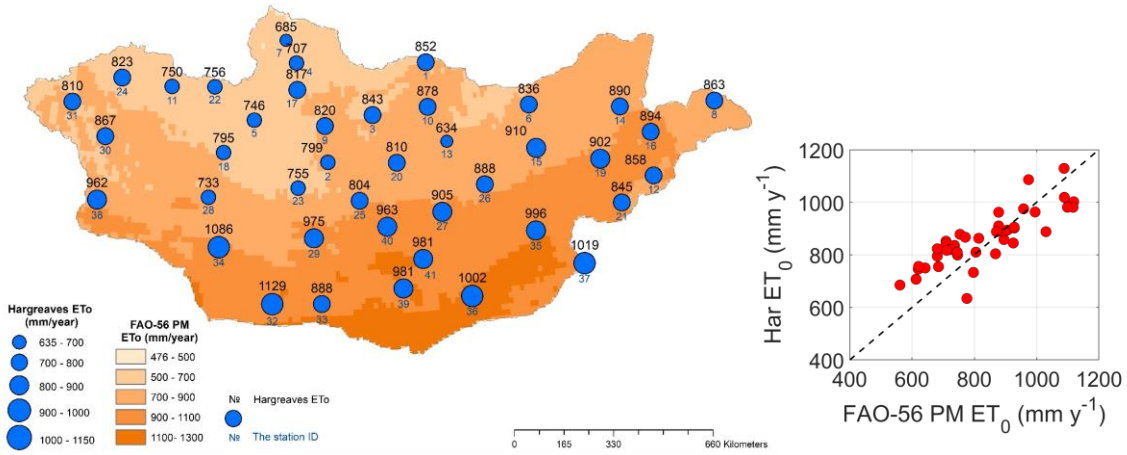

Figure 1.8. The annual mean spatial FAO-56 PM ET_o map by FAO (2009) with corresponding Har ET_o values. The plot on the right shows the comparison between FAO-56 PM ET_o and Har ET_o. Diagonal dashed line depicts the identity line (1:1 line)

This comparison of results for different periods must be taken with caution, even having similar mean and standard deviation values. As seen from the identity line, the two methods have a generally good correlation, but the performance slightly fluctuates from place to place. According to Figure 1.8, values of ET_0 tend to increase towards the south in general. The lowest annual mean ET_0 value is 634 mm, while the highest is 1129 mm.

The Har ET_0 values are compared to the corresponding FAO-56 PM ET_0 by obtaining $RMSE$=93 mm y^{-1} and R^2=0.69. Nevertheless, the Har-based ET_0 results look consistent with FAO (2009) and previous studies carried out in Mongolia (Li et al., 2007; Zorigt et al., 2012; Yu et al., 2016) and appear to form a reliable basis for further processing and modeling.

Prediction of biome-specific potential evapotranspiration, ET_p

The ET_p is calculated by multiplying ET_0 with the calculated time-variant K_c described in the Crop coefficient, K_c. Annual fluxes and corresponding aridity index, AI in 41 study locations in Mongolia are presented in Table 1.8.

Table 1.8. 5-year annual average sums of water fluxes over 41 weather stations in Mongolia

№	Stations	P (mm)	ET_0 (mm)	ET_p (mm)	E_p (mm)	T_p (mm)	AI	Class
1	Sukhbaatar	277	852	695	329	366	0.32	Semi-arid
2	Tseterleg	323	799	615	270	344	0.4	Semi-arid
3	Bulgan Mg	287	843	448	284	164	0.34	Semi-arid
4	Khatgal	277	707	449	245	204	0.39	Semi-arid
5	Tosontsengel	193	746	501	271	230	0.26	Semi-arid
6	Binder	301	836	521	297	224	0.36	Semi-arid
7	Rinchinlhumbe	193	685	428	243	185	0.28	Semi-arid
8	Khalkh gol	291	863	489	299	190	0.34	Semi-arid
9	Erdenemandal	254	820	423	269	154	0.31	Semi-arid
10	Baruunkharaa	316	878	460	298	162	0.36	Semi-arid
11	Baruunturuun	210	750	400	266	135	0.28	Semi-arid
12	Erdenetsagaan	207	858	353	233	120	0.24	Semi-arid
13	Chingis khaan (UB)	244	634	293	207	86	0.39	Semi-arid
14	Choibalsan	205	890	305	197	108	0.23	Semi-arid
15	Undurkhaan	238	910	389	291	98	0.26	Semi-arid
16	Matad	211	849	362	267	95	0.25	Semi-arid
17	Murun	227	755	323	232	90	0.3	Semi-arid
18	Uliastai	188	795	338	247	91	0.24	Semi-arid
19	Baruun-Urt	172	902	359	270	88	0.19	Arid
20	Erdenesant	246	810	308	237	71	0.3	Semi-arid
21	Dariganga	145	845	305	239	66	0.17	Arid
22	Baynuul	190	756	290	225	65	0.25	Semi-arid
23	Galuut	193	755	244	196	47	0.26	Semi-arid
24	Ulaangom	109	823	271	223	48	0.13	Arid
25	Arvaikheer	219	804	228	187	41	0.27	Semi-arid
26	Choir	111	888	237	200	38	0.12	Arid
27	MandalGobi	93	731	188	161	26	0.13	Arid
28	Altai	156	733	173	150	23	0.21	Semi-arid
29	Khoriult	95	975	247	212	35	0.1	Arid
30	Khovd	119	867	242	210	32	0.14	Arid
31	Ulgii	95	810	126	108	18	0.12	Arid
32	Ekhiingol	57	1129	159	139	20	0.05	Arid
33	Gurvantes	100	888	162	141	21	0.11	Arid
34	Tooroi	60	1086	157	137	21	0.05	Arid
35	Sainshand	109	996	148	133	16	0.11	Arid
36	Khanbogd	115	1002	174	156	18	0.11	Arid
37	Zamiin Uud	93	1019	154	138	16	0.09	Arid
38	Baitag	93	962	145	131	14	0.1	Arid
39	Dalanzadgad	128	981	176	161	15	0.13	Arid
40	Saikhan-Ovoo	113	963	147	134	13	0.12	Arid
41	Tsogt-Ovoo	79	981	239	218	21	0.08	Arid

We observe the consistent reduction of ET_0 into ET_p in accordance with the study by Zhang et al. (2012) in arid and semi-arid classes. The difference between ET_0 and ET_p increases in the Gobi Desert region, where the vegetation cover decreases (Table 1.8).

Based on the proposed dynamic method, the K_c in the steppe zone is dependent on *LAI*, while in the Gobi Desert zone, K_c is dependent on R_n. Generally, the K_c decreases from north to south. The ratio of ET_0 to P varies from 3 to 12 times in study locations, while the ratio ET_p to P is about 2.5 to 3 times. The relationship between ET_p and *LAI* is shown in Figure 1.9.

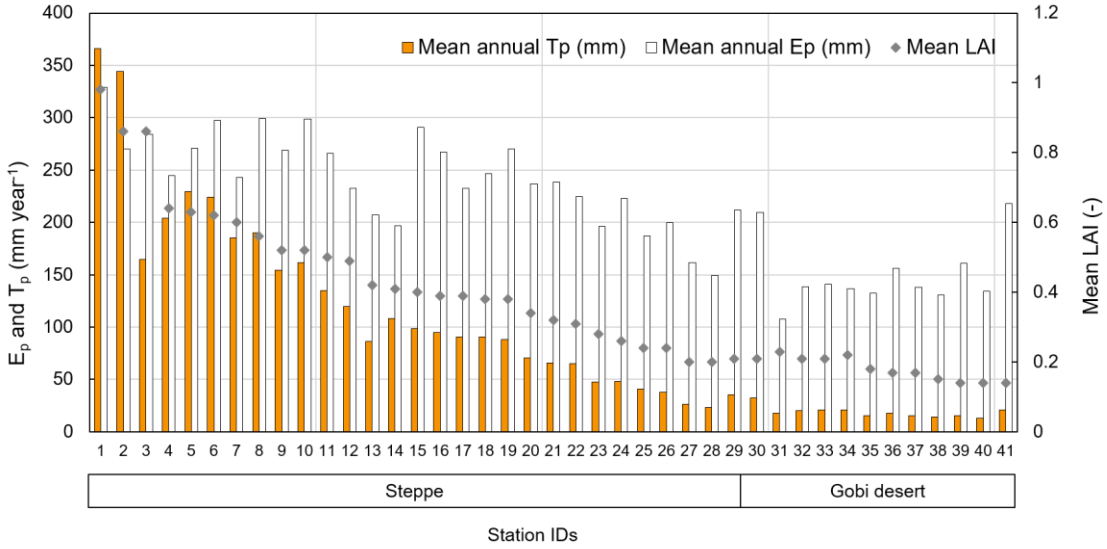

Figure 1.9. Annual average sums of E_p (white bars) and T_p (gray bars) and annual average *LAI* (orange line) over the 41 weather stations in Mongolia.

E_p constitutes a large portion of ET_p with low LAI in the southern Gobi Desert locations, while in northern Mongolia, T_p is higher, as seen from Table 1.6 and Figure 1.7. Especially in the Gobi Desert region, E_p constitutes more than 86% of ET_p over the study locations. The variations in T_p closely follow the variation in *LAI*.

The *AI* is calculated by using Har ET_0 in study locations and listed in Table 1.8. The *AI* ranges from 0.05 to 0.40. All study locations in Mongolia are categorized into the

Arid macro-class. According to Table 1.8, climate classes belong to arid to semi-arid classes in study locations. Figure 1.10 shows the aridity index values (FAO-UN AI) reported by FAO-UN (2015) developed using 1961-1990 data. The map indicates that there is an aridity gradient from north to south.

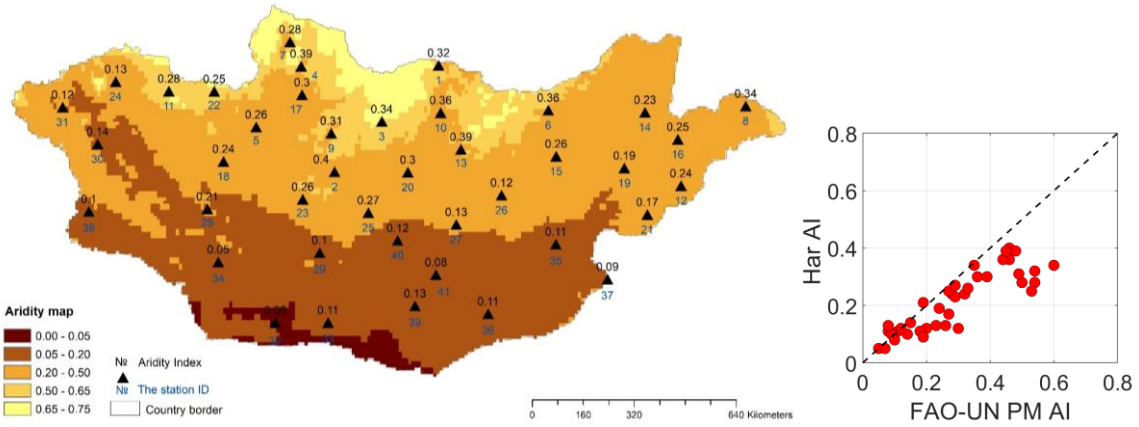

Figure 1.10. Calculated *AI* values obtained over the 41 weather stations compared to the aridity map (FAO-UN AI) extracted from the Global Aridity map (FAO-UN, 2015). The plot on the right shows the comparison between FAO-UN *AI* and Har *AI*. The diagonal dashed line depicts the identity line (1:1 line).

The calculated *AI* values are consistent with FAO-UN *AI* as shown in the map (Figure 1.10) in most study locations, especially in arid zones. Yet, Har *AI* in the northern study locations underestimates the FAO-UN *AI* values (2015) map. The discrepancy is quantified through the *RMSE*=0.11 and R^2=0.76.

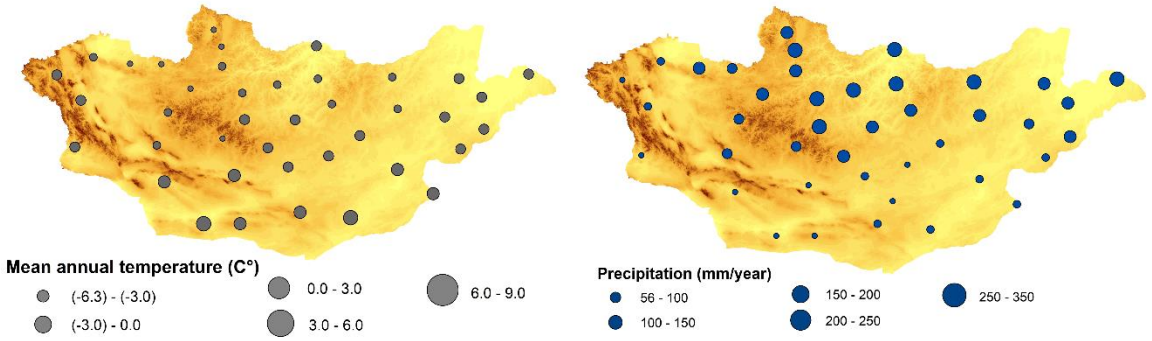

Figure 1.11. Maps showing the a) mean annual temperature and b) mean annual precipitation in study locations on DEM (Digital Elevation Model) map from SRTM (Earth Resources Observation And Science center, 2017).

The aridity increases to the south with ET_0, T increase, and P decrease (Figure 1.11). The effect of mountain ranges also can be seen, especially in the south part of Mongol-Altai and Gobi-Altai mountain ranges (Figure 1.2, Figure 1.8). The drastic differences in ET_0 are also present in the north and south of the mountain ranges, along with increased T, aridity, and decreased P patterns (Figure 1.10, Figure 1.11) in the area.

While ET_0 is higher in the Gobi Desert region due to the higher net radiation (Figure 1.12), the ET_p is now lower in the Gobi Desert Region due to its aridity, vegetation cover decrease, and vegetation stress in the region (Figure 1.12).

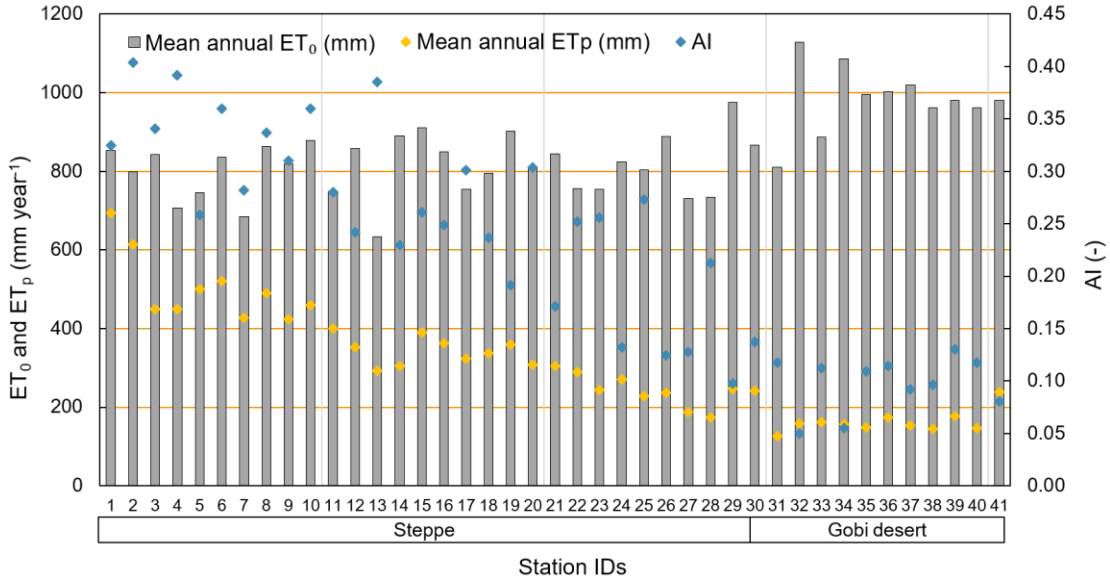

Figure 1.12.Annual average sums of ET_0 and ET_p with *AI*. Weather stations are grouped in the Gobi Desert and steppe zones

The general trend of aridity increases towards the Gobi Desert region (Figure 1.12). According to the graph, the difference between ET_0 and ET_p gets higher in the Gobi Desert and closer in the steppe. The impact of *AI* on the reduction of ET_0 into ET_p is represented by the relation between *AI* and the ratio of ET_p to ET_0 (or ET_p/ET_0) in Figure 1.13. Data are grouped according to the land cover class (Gobi Desert and steppe) and

climate class (vertical dashed line delimit arid and semi-arid climate classes, respectively). The locations belonging to the Gobi Desert (yellow circles) cluster very closely in the arid class, while the steppe points are scattered mostly in the semi-arid climate. The fit of the linear regression shows an acceptable R^2 value and describes more than 80% reduction of ET_0 in the Gobi Desert and about 54% reduction in the steppe locations under semi-arid conditions on average. Figure 1.13 shows the relationship between *LAI* and the reduction of ET_p into E_p defined by the ratio E_p/ET_p. The fit of the linear regression depicts a very high R^2 value. In the Gobi Desert, E_p constitutes almost 90% of ET_p, while in steppe zones, E_p constitutes 70% of ET_p on average. In the Gobi Desert, the potential transpiration component is marginal as manifested by low *LAI* in the growing season (Figure 1.13).

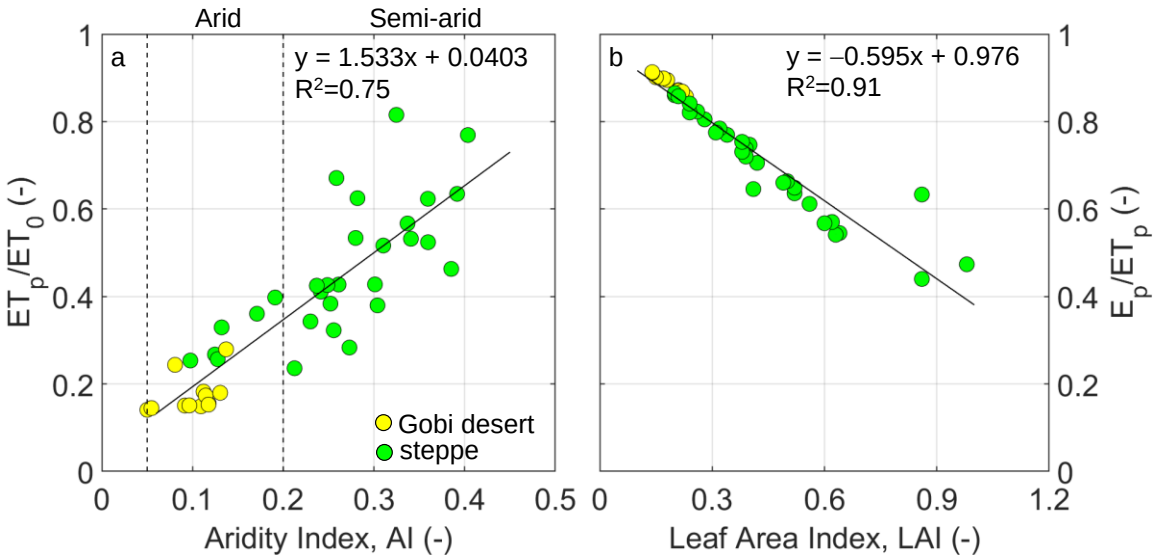

Figure 1.13. Relationships between a) aridity index, *AI* and the ratio of ET_p over ET_0, and b) leaf area index, *LAI*, and the ratio of E_p over ET_p. Solid black lines represent linear regression equations reported with associated R^2. Vertical dashed lines delimit in a) plot delimit climate classes (arid and semi-arid). The data over the 41 weather stations are grouped in Gobi Desert (yellow circles) and steppe (green circles).

Conclusions

As seen from the statistical results and cumulative comparisons, the Har shows good potential to replace FAO 56-PM method. ET_0 calculated by selected Har method tend to increase towards the south in general. The lowest annual mean ET_0 is 634 mm, while the highest is 1129 mm in the Gobi Desert.

The prediction of biome-specific potential evapotranspiration depends on the crop coefficient, K_c, which is assumed *LAI*-dependent in the steppe and radiation-dependent in the Gobi Desert zone. The estimated K_c -values decrease from north to south in the Gobi Desert. The ET_p tends to decrease to the south with the proposed K_c.

Using Beer's Law, the ET_p was partitioned to E_p and T_p using available maps of *LAI* in Mongolia. The E_p constitutes a major part of ET_p with low *LAI* in the southern Gobi Desert locations, while T_p increases toward the northern region. Results can help verify and improve the ET_p estimation methods and K_c developments in similar areas. The ET_p results will be used in the following chapter for *GR* estimation.

CHAPTER 3. THE ANALYSIS OF GROUNDWATER RECHARGE

Introduction

The *GR* will be accounted for as the infiltrated precipitation reaches the groundwater table after the ET process and capillary force effects in the vadose zone. Infiltration refers to water movement from the surface into the subsurface. In many unsaturated-zone studies, terms such as net infiltration, drainage, or percolation are used to describe water movement below the root zone, and these are often equated to recharge (Scanlon et al., 2002). Diffuse (direct) recharge refers to recharge derived from *P* or irrigation that occurs fairly uniformly over large areas, whereas focused or localized recharge refers to concentrated recharge from depressions in surface topography, such as streams, lakes, and playas (Small, 2005). Diffuse recharge is expected to be much smaller than focused recharge. However, it may be a significant component of a basin's water balance if rates are nonzero over extensive areas (Small, 2005). An example is Mongolia, with an area of 1.566.000 km^2. However, in most studies, flow processes in the unsaturated zone were not given due importance, oversimplified, or neglected due to constraints on computation resources (Rockhold et al., 1995). About the previous other studies in *GR*, the renewable groundwater resources map (that is a proxy of *GR*) was developed using the hydrograph separation method in 1982 and later updated by Jadambaa et al. (2012). It is a primary available data source for water resources planning in Mongolia. However, other than that, the studies ignore *GR* or fail to use recent methodologies. Our study focuses on estimating diffused *GR*.

GR can be estimated by using various methods depending on the scope and extent of the study. Frequently used techniques include direct measurement by lysimeters, tracer

techniques, and stream gauging (Lerner et al., 1990). However, these methods are susceptible to measurement errors and spatial variability and are often limited by their cost (Jyrkama et al., 2002; Scanlon et al., 2002). Especially in our case where the country area is so large and with a low density of human settlements in areas, it is hard to reach by a vehicle in some places. Due to the time, labor, and costs, the physical techniques are not an option. The study is also limited by data availability and consistency. The potential option for estimating *GR* is vadose-zone techniques that are applied mostly in semiarid and arid regions (Scanlon et al., 2002). The rate of *GR* in the arid areas depends on the amount of water stored and other flow processes in the vadose zone. Therefore, for accurate prediction of recharge rate, modeling the unsaturated flow process is required (Dandekar et al., 2018). A commonly used vadose zone model, HYDRUS-1D, was chosen because its accuracy has been verified by analytical techniques (Wang et al., 2009).

Based on the regional climatic features of the study and data availability, the different methods can be chosen in different functions of HYDRUS-1D. To run the model, the meteorological data and parameters of soil and vegetation are required in each location. ET_p results from Chapter 2 are used and other required datasets are shown in the following sections. In each study location, we consider a soil profile with a known thickness that separates the soil surface from the water table. By evaluating the vegetation characteristics including their root depth in Mongolia, we selected 2m-deep soil profile for all study locations in HYDRUS-1D considering availability soil data up to this depth. Our strategy is to numerically simulate the water drainage across this layer. The root zone depth (D_{rz}) in all study locations is less than 1 m. There are no other constraints for

infiltrating water after it passes the root zone. It will infiltrate towards the water table due to the gravity and traverse the entire vadose zone over some time and become *GR*. Travel time may vary depending on the actual depth to water table (D_{wt}) in study locations and will be obtained separately from *GR* and will be calculated by a simple physically-based analytical equation (Rossman et al., 2014) described in Methods.

Methods

Modeling groundwater recharge using HYDRUS-1D

The water balance in the soil-plant-atmosphere system was numerically evaluated using HYDRUS 1-D in the top 2-m-thick soil layer. This model solves the one-dimensional Richards equation (Šimůnek et al., 2008):

$$\frac{\partial\theta}{\partial t} = C(\psi)\frac{\partial\psi}{\partial t} = \frac{1}{\partial z}\partial\left[K(\psi)\left(\frac{\partial\psi}{\partial z}+1\right)\right] - \xi(z,\psi,T_p) \quad (1)$$

where t – time expressed in units of days (d),

ψ – soil pressure head (cm),

z – soil depth (positive upward) (cm),

θ – (cm^3 cm^{-3}) is soil water content,

C – (ψ) is the differential water capacity function (cm^{-1}),

ξ (z,ψ,T_p) – the sink term (d^{-1}) describing actual plant root water extraction rate function depending on z, ψ and the potential transpiration (T_p).

The numerical integration of equation (1) is performed by a finite element scheme, with computational nodes applied to the centers of a finite number of elements. The soil water retention function $\theta(\psi)$ is described by van Genuchten's equation (van Genuchten, 1980):

$$\theta(\psi) = \theta_r + \frac{\theta_s-\theta_r}{[1+(\alpha\psi^n)]^m} \quad (2)$$

where α (cm^{-1}),

m (-) and n (-) are water retention shape parameters,

θ_r (cm^3 cm^{-3}),

θ_s (cm^3 cm^{-3}) are residual and saturated water contents, respectively.

Parameters *m* and *n* are related to the Mualem's condition as *m*=1-1/*n* (Mualem, 1976). Considering the degree of saturation, $S_e=(\theta-\theta_r)/(\theta_s-\theta_r)$, which varies from 0 ($\theta=\theta_r$) to 1 ($\theta=\theta_s$), the unsaturated hydraulic conductivity function, $K(S_e)$ is given by the following equation:

$$K(S_e) = K_s S_e^l \left[1 - \left(1 - S_e^{1/m}\right)^m\right]^2 \quad (3)$$

where K_S (cm d^{-1}) – the saturated hydraulic conductivity

l – the tortuosity parameter that is assumed to be 0.5 (Mualem, 1976).

Water mass is considered mobile in the pore space delimited between the residual water content (θ_r) and saturated water content (θ_s) that correspond to null *K* and saturated hydraulic conductivity (K_s), respectively.

Pedotransfer functions

Soil hydraulic properties control soil mosture movement described by the Richards equation (Equation 1) and includes all the hydrological processes occurring in the vadose zone, namely the infiltration, runoff, drainage, and soil surface evaporation, together with root water uptake. Depending on the soil type, the same amount of moisture content can have a different amount of water available for the plant (Radcliffe and Simunek, 2010). Thus, the understanding of soil water potential and building the soil water retention curve is one of the important steps of the study. However, the parameterization based on in situ data collection is quite time-consuming and expensive.

The application of vadose zone models is usually restricted by finding these parameters, especially because of a lack of in-situ soil hydraulic characteristics (SHCs) (Wösten et al., 2001). In response, the soil science community has developed

pedotransfer functions (PTFs), which estimate soil hydraulic properties from easily measured soil attributes, such as soil texture, organic carbon, and oven-dry bulk density (van Genuchten, 1980; Bouma, 1989; Yonggen Zhang & Schaap, 2017b).

PTFs have been widely used to predict soil hydraulic parameters in favor of expensive laboratory or field measurements (Yonggen Zhang & Schaap, 2017a). Most PTFs estimate parameters of empirical hydraulic functions with modest accuracy (Zhang & Schaap, 2017a) when available from generalized regional data. Since PTFs show promising results in description of soil hydraulic parameters used in the HYDRUS-1D model, the one with the closest geographical and climatic background can be implemented in the study. Recently, some PTFs have been obtained for the Gobi and other border regions with China. The attempt to use this PTF (Liao et al., 2011) has been implemented, however the soil hydraulic results were not reliable. Thus, the Rosetta built in PTF in HYDRUS will be used for the study.

Rosetta (Schaap et al., 2001) denoted as Rosetta1, is one of many PTFs and is based on artificial neural network (ANN) analysis coupled with the bootstrap resampling method, which allows the estimation of van Genuchten water retention parameters (van Genuchten, 1980), (abbreviated here as VG), saturated hydraulic conductivity (K_s), and their uncertainties (Zhang & Schaap, 2017b). Table 2.2 shows the soil properties in each station as well as soil hydraulic results obtained from Rosetta in HYDRUS-1D.

Net precipitation

The rainfall interception *RI* has calculated as shown in the following equation (Nasta & Gates, 2013).

$$RI = aLAI\left(1 - \frac{1}{1+\frac{bP}{aLAI}}\right) \quad (4)$$

where a (cm/d) is an empirical coefficient, assumed as 0.025 cm/d and b (-) denotes the soil cover fraction given by:

$$b = 1 - e^{-kLAI} \quad (5)$$

Interception is subtracted from the measured rainfall in order to obtain the net rainfall P that has been calculated in study locations and used as the HYDRUS-1D input.

Root water uptake

Most terrestrial plants exert root water uptake from the vadose zone. Plants wilt when soils become too dry because the forces holding the water in the soil are too strong to allow the plants to maintain a pressure gradient with lower pressure inside the root. Understanding the movement of soil water, and its uptake by plants, and "loss" through evapotranspiration and recharge to the groundwater system, is essential (Patricia et al., 2015).

The sink term, S, is defined as the volume of water removed from a unit volume of soil per unit time due to plant water uptake. (Feddes, 1978) defined ξ as

$$\xi(\psi) = \alpha(\psi)T_p \quad (6)$$

Where the root-water uptake water stress response function $\alpha(\psi)$ is a prescribed dimensionless function of the soil water pressure head ($0 \leq \alpha \leq 1$), and T_p the potential water uptake rate (potential transpiration). Water uptake is assumed to be zero close to saturation (i.e., wetter than some arbitrary "anaerobiosis point", ψ_1). For $\psi < \psi_4$ (the wilting point pressure head), the water uptake is also assumed to be zero. Water uptake is considered optimal between pressure heads ψ_2 and ψ_3, whereas for pressure heads between ψ_3 and ψ_4 (or ψ_1 and ψ_2), water uptake decreases (or increases) linearly with ψ.

The variable T_p in is equal to the water uptake rate during periods of no water stress when $\alpha(\psi)=1$ (Figure 2.1).

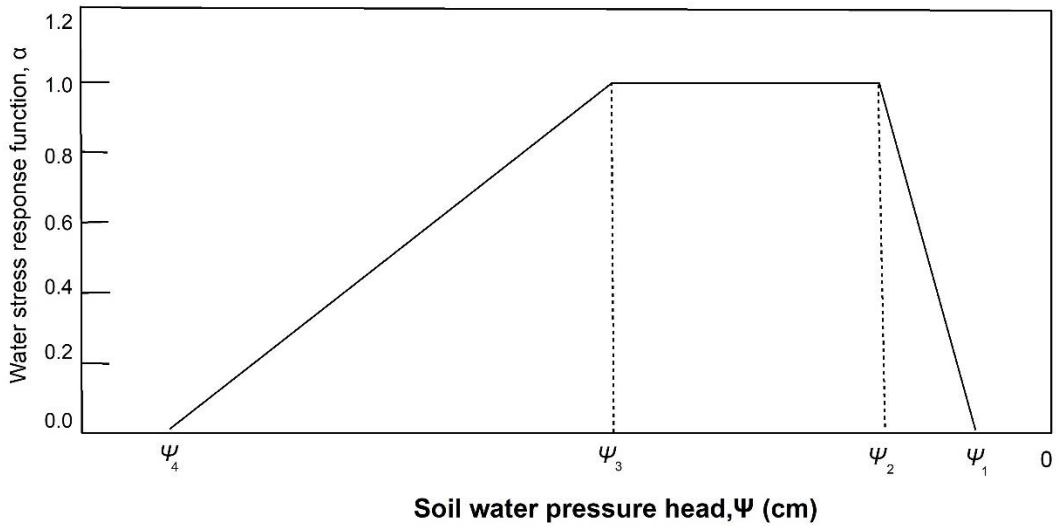

Figure 2.1. Schematic of the plant water stress function, $\alpha(\psi)$ by (Feddes, 1978)

Comparing Groundwater recharge with existing groundwater recharge map

In general, the groundwater recharge in Mongolia is small and often is entirely neglected when this component of the water budget is negligible compared with *P* (Nandintsetseg et al., 2010). There is one main study addressing the groundwater recharge in Mongolia developed by Jadambaa et al. (2012). Using "Regional Hydrogeological Map of Mongolia, Multi-year Mean Flow of Surface Water and Groundwater" at the scale of 1:1.000.000, aquifer information, and borehole information, they developed the Renewable Groundwater Resource map.

The Map of "Multi-year Mean Flow of Surface Water and Groundwater" at the scale of 1:1,000,000 was created and printed in Aero-Geology Research Institute in Moscow, Russian Federation in 1981 (Aerogeology Research Institute in Moscow, 1981). The map shows the surface water runoff as contours and the groundwater flow as

polygons. The groundwater flow polygons represent the total flow that originates from groundwater flow and infiltration of surface water and precipitation and presented in mm/year. Therefore, the map is also sometimes described as a groundwater flow map. The groundwater flow indicated on the map corresponds to the renewable (or natural) groundwater resources. This map obtained from stream gaging, spring analysis, and hydrograph separation was used over 40 years for state planning.

The renewable groundwater resource map (Figure 2.10) has developed from the groundwater flow resources of the area, composed of lateral groundwater flow and recharge from infiltration of surface water and precipitation on 1:1,000,000 "Multi-year Mean Flow of Surface Water and Groundwater" Map in mm/year was converted into m^3/day as follows:

$$Q = 2.74HF \tag{7}$$

where Q – groundwater renewable resource (m^3/day),

H – groundwater resource (mm/year),

F – flow area, km^2.

Legend presents a classification of the natural resources per 1 km^2 as follows: <5 mm/year, 5-10 mm/year, 10-20 mm/year, 20-50 mm/year, 50-100 mm/year, 100-200 mm/year, and >200 mm/year (Jadambaa et al., 2012). Our *GR* results will be compared with this map with consideration of its methodology.

Vadose zone lag time

It is important to remember that drainage rates in thick unsaturated zones do not always reflect current recharge rates at the water table (Scanlon et al., 2002). Annual average drainage in HYDRUS-1D in the top 2-m-thick soil layer is equal to potential *GR*

infiltrating to the bottom soil layer with depth Z_{bot}. According to (Rossman et al., 2014), vadose zone lag time can be calculated using depth to water table and vertical soil moisture velocity (c). The equation for c is expressed as:

$$c = \frac{dK(\theta)}{d\theta} = \frac{K_s(1-S_f^m)}{2(\theta_s-\theta_r)S_e^{1/2}}\left[1 + \frac{4S_e^{1/m}S_f^{m-1}}{(1-S_f^m)}\right] \quad (8)$$

where S_f is:

$$S_f = 1 - S_e^{1/m} \quad (9)$$

Once c had been determined from Equation 6, the lag time can be computed as follows:

$$\tau = Z_{bot}/c \quad (10)$$

where Z_{bot} is the mean depth to the water table or vadose zone thickness excluding root zone and can be computed as follows:

$$Z_{bot} = D_{wt} - D_{rz} \quad (11)$$

where D_{wt} – the mean depth to the water table or vadose zone thickness.

D_{rz} – Root zone depth.

Data collection

The collected in study locations dataset and data sources are shown in the following table.

Table 2.1. Data sources

Collected data/parameters	Unit	Period of data availability	Source	References
Daily *P*	mm	2007-2011	NAMEM	(National Agency for Meteorology and Environmental Monitoring)
Daily E_p and T_p	mm	2007-2011	Study results from chapter 2	
Soil physical properties (Sand percentage, Silt percentage, Clay percentage, Bulk density)	%,	-	ISRIC – World Soil Information	(van den Bosch & Batjes, N, 2013)
Depth to the water table	m	-	Hydrogeological maps	(Mineral Resources and Petroleum Authority, 1994)

The detailed information about datasets is shown in the following sections.

Biome-specific potential Evapotranspiration

The ET_p has been calculated from Har ET_0 and K_c in study locations. Then ET_p values have been partitioned into daily values of E_p and T_p using Beer's law as shown in Chapter 2 in each study location.

Soil hydraulic parameters

In order to use the PTFs, there is a need to collect soil physical properties in the study locations. However, there are no accessible measured data in these locations; thus, the remote sensing products have been explored. The most data-rich and reliable source

was Soilgrids (Van Den Bosch and Batjes, 2013), and therefore this data product was used for the study. SoilGrids is a system of global digital soil mapping that uses state-of-the-art machine learning methods to map the spatial distribution of soil properties across the globe. SoilGrids prediction models are fitted using over 230,000 soil profile observations from the WoSIS database and a series of environmental covariates (Van Den Bosch and Batjes, 2013). Covariates were selected from a pool of over 400 environmental layers from Earth observation-derived products and other environmental information, including climate, land cover, and terrain morphology. The outputs of SoilGrids are global soil property maps at six standard depth intervals (according to the GlobalSoilMap IUSS working group and its specifications) at a spatial resolution of 250 meters. Prediction uncertainty is quantified by the lower and upper limits of a 90% prediction interval (Van Den Bosch and Batjes, 2013). The soil physical properties up to 200 cm in 6 soil intervals have been collected from Van Den Bosch and Batjes (2013) and prepared as input for Rosetta in HYDRUS-1D.

Root zone

The sink term ξ is defined as the volume of water removed from a unit volume/depth of soil per unit time due to the plant water uptake (Šimunek, 2015). The major root zone was identified as a 30 cm soil layer (Yanagawa et al., 2015) in Mongolia. However, some of the species commonly have a well-developed root system. Most often, one finds *Haloxylon ammodendron*, *Nitraria sphaerocarpa*, and less often *Tamarix ramosissima*. The Ekhiin gol and Tooroi study locations are covered with *Haloxylon ammodendron* nearby thus the root depth of 97 cm has been set for this specific

vegetation according from (Wang et al., 2017). The root zone in other study locations are considered as a 30 cm soil layer.

Soil moisture

Soil moisture is an important variable that characterizes water balance of hydrological processes occurring within the groundwater-soil-plant-atmosphere system (Robock et al., 2000). Furthermore, soil moisture regulates the ratio of runoff and infiltration and controls major energy fluxes (Natsagdorj et al., 2019).

However, the soil moisture is not systematically measured or accessible in Mongolia agencies, except for remote sensing sources (Robock et al., 2000). Only Nandintsetseg and Shinoda (2011) and Nandintsetseg and Shinoda (2014) provide substantial analysis of soil moisture status in different natural zones in Mongolia is avavilable. However, time-variable θ measurements for using directly in HYDRUS-1D are unavailable at study locations.

Remote sensing techniques are increasingly used for monitoring surface soil-moisture conditions over large areas, but extending surface soil moisture to the root zone is still facing some limitations, especially when no time-series observations are available, which is very common in practice (Zeng et al., 2017).

The soil moisture data were taken from https://ismn.geo.tuwien.ac.at/en/ (Dorigo et al., 2011) for several stations in Mongolia between 1975 to 2002. The measurement frequency was variable, and most data are available in province center weather stations. The θ measurements are collected for few study locations to test whether the data is reliable (Annex 3.1). The results have been used to set up the initial θ through the soil profile in HYDRUS-1D and checked whether the final θ are in the range from the data;

however, some anomaly results are observed. As seen from the results, data might not be correct in site-specific studies; therefore, site-specific calibration is required. Thus, the result is considered not to be reliable and no soil moisture data has used for HYDRUS-1D in the study.

Depth to the water table

The water table data in parts of Mongolia have been obtained from available maps (Mineral Resources and Petroleum Authority, 1994), but have substantial uncertainty. The collected depths to the water table are shown in Annex 3.2. The unknown depths to water table in some locations are assigned at 10 m.

HYDRUS-1D setup

Over the 41 study sites, we set the depth of the 2 m soil layer for all study locations which is assumed adequate depth that passes the root zone. The upper boundary condition is subject to measured (net P) and estimated (E_p) fluxes monitored by the weather station. P and E_p represent the system-dependent time-variable daily water fluxes of the upper boundary condition. The lower boundary condition is set to free drainage.

The partitioned E_p and T_p from Chapter 2 and net P are used as input data for upper boundary. T_p determines the potential root water uptake (sink term in the Richards equation). Root distribution is assumed to be linear along with the soil profile by varying from maximum at the soil surface to minimum at maximum root depth which are 30 cm or 97 cm depending from the location. Both E_p and T_p are reduced by water limitation into actual evaporation (E_a) and actual transpiration (T_a). The actual root water extraction rate ξ is modeled according to Feddes et al. (1978). HYDRUS 1-D includes a dataset of specific-crop root water stress parameters. The transpiration efficiency function (between 0 and 1) depends on the soil pressure head. In our case, the vegetation is chosen as pasture in study locations in HYDRUS-1D. For this pasture, the wilting point corresponds to -8000 cm (Figure 2.1.) in HYDRUS-1D.

The soil physical properties are used to obtain soil hydraulic parameters in study locations. Due to the absence of soil moisture data, initial condition set by approximate value and the spin-up method used to diminish the effect from initial condition. The short configuration of study locations are shown below.

The HYDRUS-1D configuration

The HYDRUS-1D configuration in study locations is set as shown in the following.

Main processes	Water flow, Root water uptake
Boundary conditions	Upper boundary: Atmospheric BC with Surface runoff
	Lower boundary: Free drainage
Initial conditions	39% of θ_s through the 200 cm soil profile
Soil profile depth	200 cm
Root zone depth	30 or 97 cm

Due to the absence of soil temperature data, the winter freezing effect has not been calculated.

Setting initial condition and spin-up

Reliable numerical simulation of soil water movement requires accurate determination of model parameters as well as initial and boundary conditions. However, the accurate initial soil moisture or matric potential along with the soil profile at the beginning of simulation time is unavailable, making it necessary to run the simulation model from the arbitrary initial condition until the uncertainty of the initial condition (UIC) diminishes (Yu et al., 2019). The spin-up method will be used for running a model using our 5-year data repeatedly. The number 5-year cycles is run repeatedly until the model output adjusts from the initial conditions to a realistic soil moisture profile where the water and energy budgets are balanced, and there is minimal drift in model state variables or prognostic variables (Ajami et al., 2014). After completion of these model spin-ups, the model should contain a physically realistic state of equilibrium between the external forcing and the simulated water fluxes.

The initial soil moisture set by observing the various runs with different initial condition. When the initial condition being closer to final equilibrated soil moisture, the

lesser number of 5-year cycles will be required. And in order make the initial soil condition as close to final equilibrated soil moisture, the 39 % of θ_s is proposed to be used as initial condition the soil profile in all study locations uniformly.

Due to the initial condition set-up, soil hydraulic parameters, and other factors, the study locations can have different number of 5-year cycles. Thus, the study locations have been categorized into groups based on the soil hydraulic conductivity, texture type, and aridity index to get an idea of how many repetitions are needed. The main parameters to group the study locations are shown in Table 2.2.

Table 2.2. The main parameters of study locations

ID	Study locations	Aver K_s, (cm/d)	Aver θ_s, (cm/d)	Texture	*AI*	Class
1	Sukhbaatar	23.13	0.43	Loam	0.37	Semi-arid
2	Tsetserleg	15.3	0.42	Loam	0.44	Semi-arid
3	Bulgan	17.22	0.42	Loam	0.41	Semi-arid
4	Khatgal	29.13	0.46	Sandy clay loam	0.45	Semi-arid
5	Tosontsengel	19.2	0.43	Loam	0.34	Semi-arid
6	Binder	22.19	0.42	Loam	0.42	Semi-arid
7	Rinchinlhumbe	32.37	0.46	Sandy loam	0.41	Semi-arid
8	Khalkh gol	15.62	0.41	Loam	0.39	Semi-arid
9	Erdenemandal	16.26	0.43	Loam	0.36	Semi-arid
10	Baruunkharaa	18.59	0.41	Loam	0.42	Semi-arid
11	Baruunturuun	21.19	0.44	Loam	0.29	Semi-arid
12	Erdenetsagaan	12.39	0.42	Loam	0.28	Semi-arid
13	Chingis khan	18.6	0.41	Loam	0.35	Semi-arid
14	Choibalsan	11.16	0.4	Loam	0.27	Semi-arid
15	Undurkhaan	12.05	0.41	Loam	0.33	Semi-arid
16	Matad	17.2	0.4	Loam	0.28	Semi-arid
17	Murun	15.75	0.44	Loam	0.31	Semi-arid
18	Uliastai	16.52	0.42	Loam	0.27	Semi-arid
19	Baruun-Urt	11.23	0.41	Loam	0.23	Semi-arid
20	Erdenesant	15.69	0.41	Loam	0.29	Semi-arid
21	Dariganga	16.15	0.41	Loam	0.16	Arid
22	Bayan-Uul	21.63	0.43	Loam	0.26	Semi-arid
23	Galuut	20.29	0.42	Loam	0.3	Semi-arid
24	Ulaangom	16.78	0.43	Loam	0.15	Arid
25	Arvaikheer	12.92	0.41	Loam	0.3	Semi-arid

26	Choir	11.87	0.42	Loam	0.15	Arid
27	MandalGobi	12.35	0.41	Loam	0.12	Arid
28	Altai	13.71	0.42	Loam	0.23	Semi-arid
29	Khoirult	13.57	0.4	Loam	0.09	Arid
30	Khovd	12.92	0.42	Loam	0.15	Arid
31	Ulgii	17.31	0.42	Loam	0.13	Arid
32	Ekhiingol	8.82	0.42	Silt loam	0.05	Hyper-arid
33	Gurvantes	11.59	0.4	Loam	0.1	Arid
34	Tooroi	11.34	0.44	Loam	0.05	Hyper-arid
35	Sainshand	8.34	0.4	Silt loam	0.13	Arid
36	Khanbogd	9.9	0.39	Silt loam	0.1	Arid
37	Zamiinuud	8.93	0.4	Silt loam	0.15	Arid
38	Baitag	12.27	0.41	Loam	0.11	Arid
39	Dalanzadgad	14.22	0.39	Loam	0.15	Arid
40	Saikhanovoo	11.49	0.4	Loam	0.15	Arid
41	Tsogt-Ovoo	10.82	0.41	Loam	0.1	Arid

The study locations are divided into groups based on its similarity of conditions shown in Table 2.2. The following texture and aridity index combination (Table 2.3) are chosen to represent these groups, and its result will be used to identify spin-up repetition.

Table 2.3. Texture and *AI* class

Texture	AI class	Chosen station to represent
Sandy loam	Semi-arid	Rinchinlhumbe
Sandy clay loam	Semi-arid	Khatgal
	Semi-arid	Tsetserleg
Loam	Arid	Dariganga
	Hyper arid	Tooroi
Silt Loam	Arid	Khanbogd
	Hyper arid	Ekhiin gol

Each repetition of the HYDRUS-1D computations in spin-up consists of 5-year dataset. The same number of repetitions was used in other locations from the same soil texture and aridity combination. If needed, the additional repetitions were conducted in some study locations. The volumetric water content dynamics at the bottom of the simulated depth from spin-ups are presented in the following graphs.

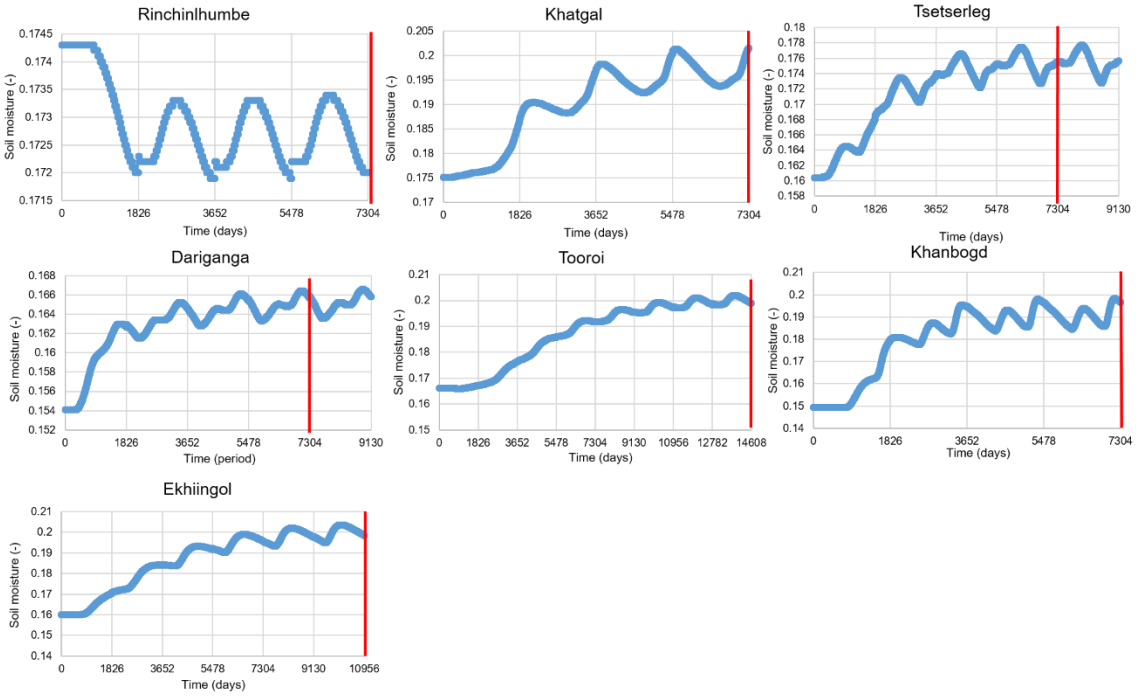

Figure 2.2. Soil moisture at the bottom spin ups

Generally, spin-up time increases when the soil is more fine-textured, drier, or located in higher aridity locations (Figure 2.2). In addition, the repetition of times depends on how the initial soil moisture has set. The spin-ups stopped when the soil moisture at the beginning of each cycle becomes repetitive or becomes small. Those spin-up repetitions are used to run the study locations from the same combination of initial conditions and duo in HYDRUS-1D. In the study locations, which could not be equilibrated during identified spin-ups, additional spin-ups will be conducted on a case-by-case basis. The volumetric water content or pressure head results at the end of each spin-up in study locations are used to set initial conditions in actual runs.

Results and discussion

Actual evapotranspiration result, ET_a

Five-year dataset 2007-2011 with improved initial conditions from spin-ups has been used for the runs. The water balance results are obtained from HYDRUS-1D output text files in study locations. These results will be used to understand how the *P* partitions into ET_a and *GR* in study locations. In Chapter 1, we calculated ET_p and used it as one of the inputs in HYDRUS-1D. The following graph shows mean annual ET_0, ET_p, and E_a, T_a results from HYDRUS-1D.

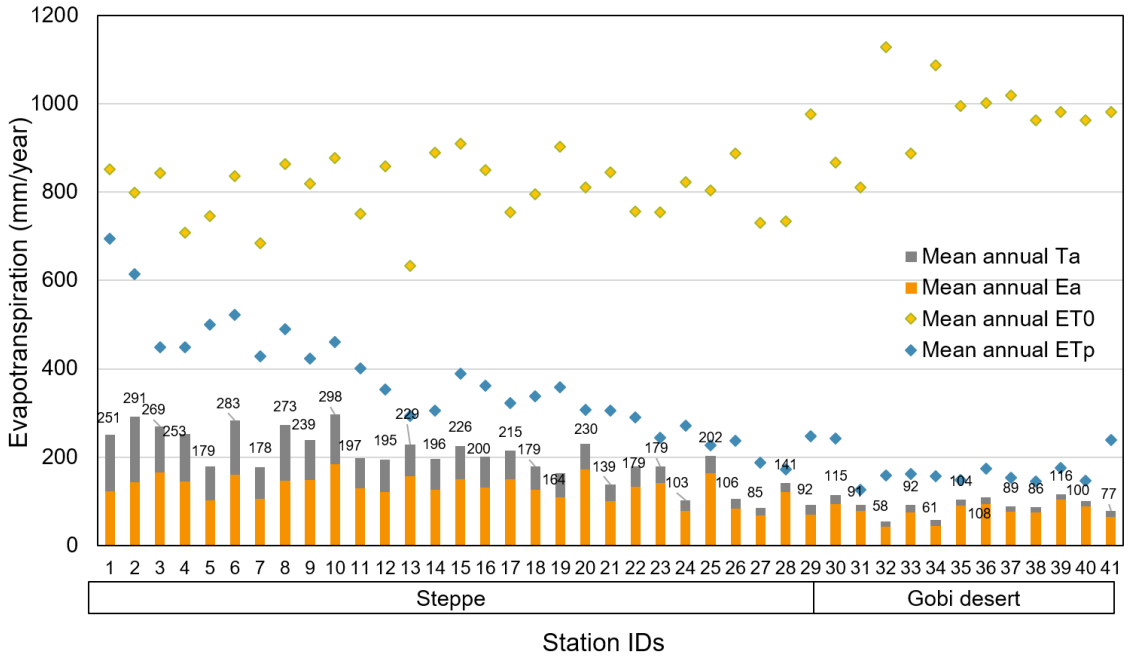

Figure 2.3. Overall ET results in study locations

As seen from the graph, ET_0 increases to the south towards the Gobi region. With consideration of natural zone and soil water stress conditions, the ET_p were calculated from using K_c in study locations that were developed in Chapter 2. It can be seen that the general trend of ET_p follows ET_a.

Analyses of the ET_a indicate that the T_a constitutes a major part in steppe regions with higher *LAI*, while it decreases towards the Gobi region. In the study location in the Gobi regions, E_a constitutes from 71 to 89 % of ET_a. Generally, it can be clearly seen that ET_a follows *LAI* trends (Figure 2.4).

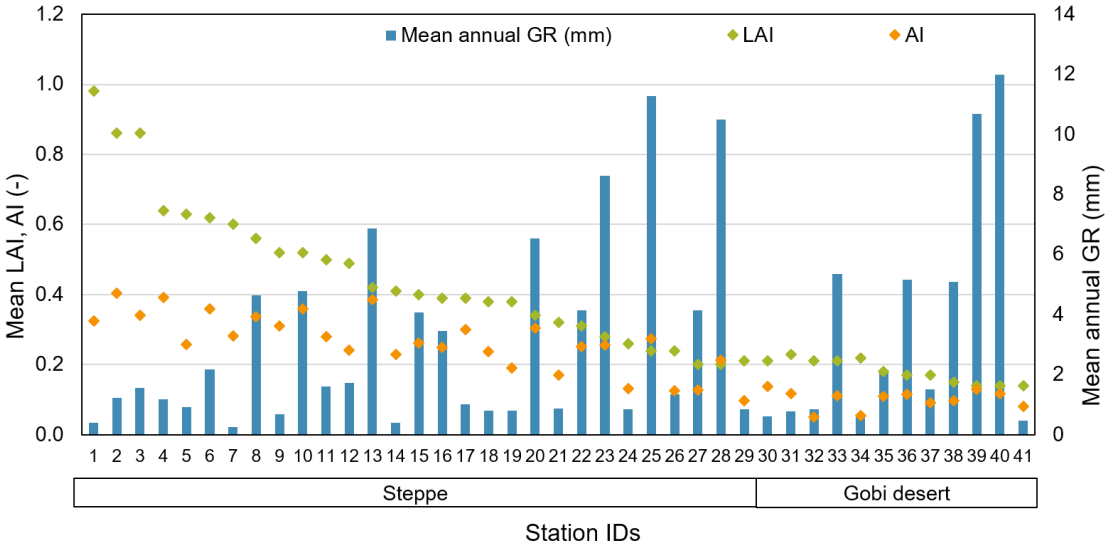

Figure 2.4.Trends in mean annual ET_a and *LAI*, and *AI*

Calculated results for ET_a in study locations and the ET_a map by FAO (2009a) obtained from the one-dimensional water balance method are presented in Figure 2.5.

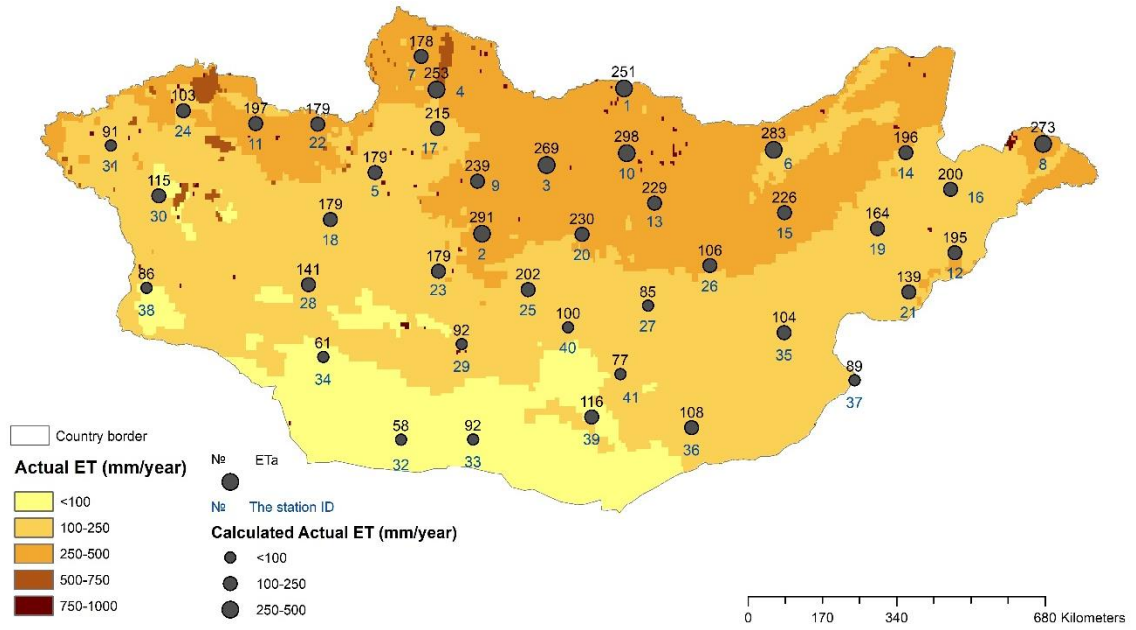

Figure 2.5. Comparison of values of actual annual ET_a obtained from HYDRUS-1D one- dimensional soil-water balance method prepared by FAO (FAO, 2009a) on the map with a spatial resolution of 5 arc minutes.

The highest mean annual ET_a is 298 mm in Tsetserleg (ID 10), while the lowest is 58 mm in Ekhiin gol (ID 32) as shown in Figure 2.5. Our ET_a from HYDRUS-1D matches well in three most study locations in the southern part, where ET_a is lower than 250 mm. However, in the northern part, the FAO map seems like overestimate of the ET_a. The overestimation was also observed earlier in ET_0 and *AI* maps by FAO in Figure 1.10.

Groundwater recharge rates

While the previous part presents the ET_a results, Figure 2.6 shows how *P* partitions into ET_a and *GR*.

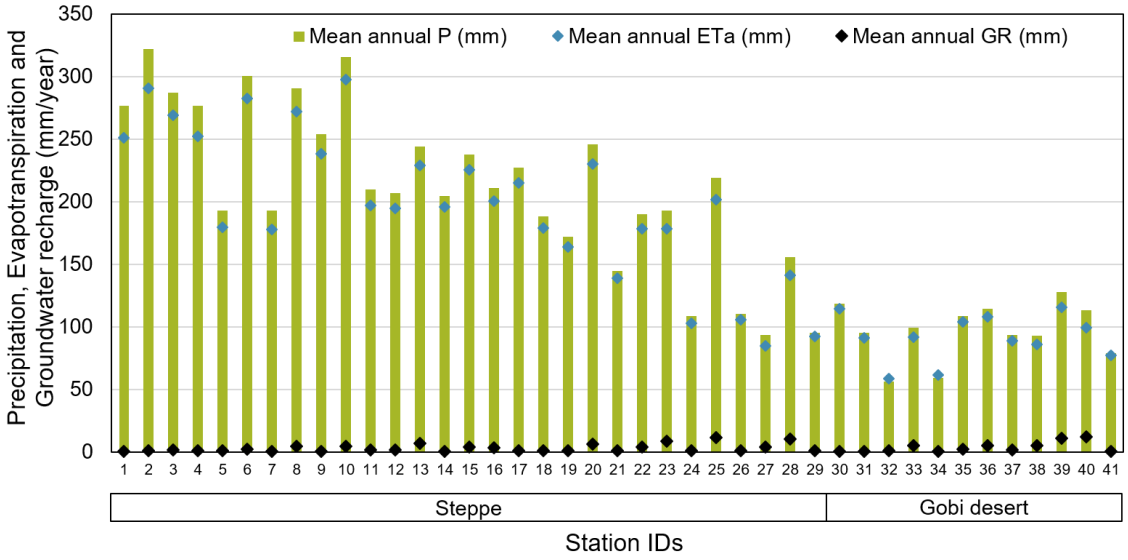

Figure 2.6. Precipitation, evapotranspiration, and groundwater recharge (mm/year), obtained from Hargreaves equation for ET_p and reduced K_c

The *P* was lower than the infiltration capacity of soil in study locations; thus, the runoff was 0 in all study locations. The runoff can be better represented in regional hydrology models in Mongolia. The country is located in high elevations, windy, and with very limited *P* throughout the country. The soil is dry during most of the year (Nandintsetseg & Shinoda, 2011), the *P* tends to become ET_a, and there is very little left to percolate. ET_a constitutes more than 88 % of *P* in all study locations. The *GR* constitutes only up to 11 % of *P* (highest 11% at Saikhanovoo (ID 40)) in study locations. The following table shows the yearly *GR* and *P* in the study period.

Table 2.4. *GR* and *P* (mm/year)

ID	Stations	Yearly *GR* (mm/year)					Mean annual *GR* (mm/year)
		2007	2008	2009	2010	2011	
1	Sukhbaatar	0.4	0.4	0.4	0.4	0.4	0.4
2	Tseterleg	1.2	1.4	1.3	1.1	1.2	1.2
3	Bulgan Mg	1.8	1.8	1.6	1.3	1.4	1.6
4	Khatgal	1.5	1.2	1.0	0.9	1.2	1.2
5	Tosontsengel	1.2	1.2	0.9	0.7	0.6	0.9
6	Binder	2.0	1.5	2.0	2.7	2.7	2.2
7	Rinchinlhumbe	0.3	0.4	0.3	0.3	0.1	0.3
8	Khalkh gol	5.5	4.4	4.6	4.6	4.1	4.6

9	Erdenemandal	0.6	0.7	0.8	0.7	0.7	0.7
10	Baruunkharaa	2.9	4.5	6.7	5.5	4.3	4.8
11	Baruunturuun	2.1	1.7	1.4	1.2	1.7	1.6
12	Erdenetsagaan	2.4	1.5	1.8	1.9	1.0	1.7
13	Chingis khaan (UB)	4.5	4.4	8.8	10.7	5.9	6.9
14	Choibalsan	0.4	0.4	0.4	0.4	0.4	0.4
15	Undurkhaan	5.8	3.9	3.0	3.8	3.8	4.1
16	Matad	4.7	3.6	3.4	2.9	2.6	3.4
17	Murun	1.2	1.0	0.9	1.0	1.0	1.0
18	Uliastai	0.9	0.8	0.8	0.7	0.8	0.8
19	Baruun-Urt	0.7	0.9	0.9	0.8	0.7	0.8
20	Erdenesant	13.0	6.3	4.2	3.3	5.9	6.5
21	Dariganga	0.8	0.8	0.9	0.9	1.0	0.9
22	Baynuul	4.9	2.9	2.9	3.9	6.2	4.1
23	Galuut	20.9	9.1	4.1	3.2	5.9	8.6
24	Ulaangom	1.0	0.9	0.8	0.7	0.8	0.8
25	Arvaikheer	17.3	16.2	10.2	5.9	6.7	11.3
26	Choir	1.5	1.6	1.3	1.1	1.1	1.3
27	Mandalgobi	5.3	3.0	2.0	1.7	8.7	4.1
28	Altai	17.1	9.1	5.6	3.8	16.9	10.5
29	Khoriult	0.9	0.8	0.8	0.8	0.9	0.8
30	Hovd	0.7	0.7	0.6	0.5	0.5	0.6
31	Ulgii	0.9	0.8	0.8	0.7	0.7	0.8
32	Ekhiingol	0.8	0.8	1.2	1.2	1.0	1.0
33	Gurvantes	2.5	8.1	8.6	4.7	2.9	5.3
34	Tooroi	0.7	0.7	0.8	0.8	0.7	0.7
35	Sainshand	2.3	2.5	1.9	1.9	1.9	2.1
36	Khanbogd	5.8	3.9	5.4	4.3	6.3	5.2
37	Zamiin Uud	1.5	1.5	1.5	1.5	1.5	1.5
38	Baitag	5.6	4.2	3.1	4.8	7.7	5.1
39	Dalanzadgad	11.2	13.0	12.2	6.0	11.0	10.7
40	Saikhan-Ovoo	4.6	21.4	20.9	8.4	4.7	12.0
41	Tsogt-Ovoo	0.5	0.5	0.5	0.5	0.5	0.5

GR varies through the 5 years; however, it was not directly related to the higher *P* rate in a particular year. The fluctuation over the years in study locations varies. In a spatial average of all study locations, 2011 had the highest *P* and 2007 had the least *P*, while about the *GR*, the highest observed in 2007 and least observed in 2010. The variability of hydrometeorological and hydrogeological conditions is believed to strongly control whether diffuse recharge occurs; precipitation *P* rate may exceed the ET_p over some interval, even though $P/ET_p < 1$. According to our yearly *P* and *GR* rates, there has

not direct *GR* effect been observed in years with higher *P*. However, the occurrence of a single large precipitation event or a series of events may yield diffuse recharge (Barnes et al., 1994; Stephens, 1994). According to our results, the *GR* was cumulative of many small recharge events through the year rather than several large *GR* events. For example in the Sukhbaatar station, where we have highest *P* rate, there was no peak *GR* observed with higher *P* rate. Since the *GR* results are so small, it was hard to distinguish whether which *P* event caused more *GR*, but the soil moisture fluctuates due to the *P*, which certainly impacts *GR*.

Second, the presence and type of vegetation are believed to play a key role in controlling diffuse recharge. At sites in New Mexico and Nevada, Gee et al. (1994) found that water accumulated in deep lysimeters kept vegetation-free, whereas deep percolation did not occur in lysimeters the same sites with growing vegetation. Desert vegetation, such as the shrub *Larrea* (Creosote bush), have relatively deep root systems (David and Vokhmin, 2002) and transpires until soil water potential is highly negative (-8 MPa) (Pockman and Sperry, 2000). Recharge is generally much greater in non-vegetated than in vegetated regions (Gee et al. 1994) and greater in areas of annual crops and grasses than in areas of trees and shrubs (Adane et al., 2018; Prych, 1998; Scanlon et al., 2002). According to our results, the same pattern has been observed, and it can be seen in Figure 2.7.

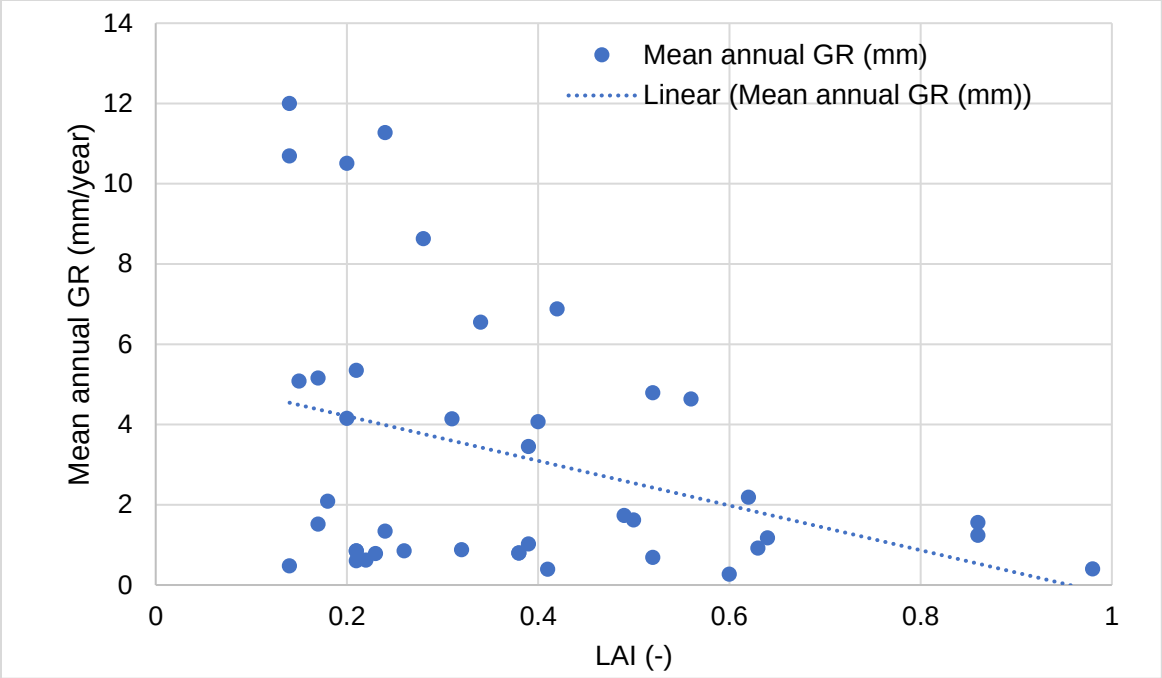

Figure 2.7. The *LAI* vs. *GR* in study locations

In areas with higher *P*, there is most likely more vegetation, which results in higher transpiration. Thus, in those stations, there was very small *GR* observed in more vegetated areas where the *LAI* is higher. Therefore, an inverse relationship has been observed between *LAI* and *GR* (Figure 2.7). However, in the Gobi Desert study, locations with deeper root systems Ekhiingol (ID 32) and Tooroi (ID 34) have a smaller *GR* than other Gobi Desert study locations. The two stations have *P* less than mean annual 100 mm/year, and they have saxaul vegetations (*Haloxylon ammodendron*). With their deeper root depth, they extract most of the available water in the soil and leave almost none to percolate.

Third, the diffuse recharge is expected to be greater through coarse soils than fine soils because wetting fronts propagate more deeply into coarse soils (Small, 2005). The following figure shows the relationship between *GR* rates (mm/year) and soil texture as a fraction of sand (%), silt (%), and clay (%).

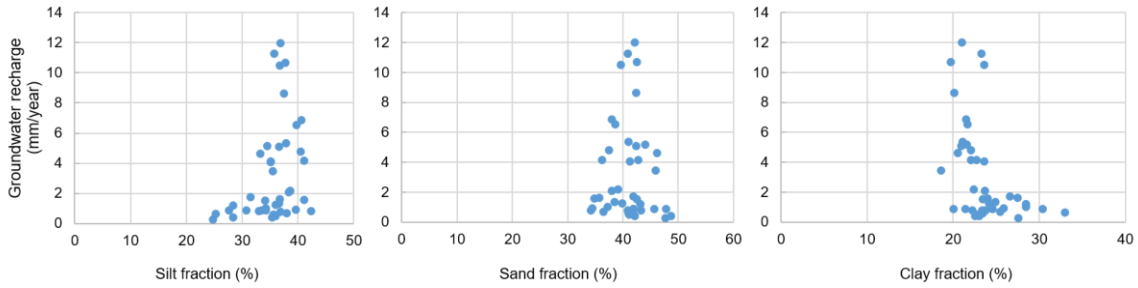

Figure 2.8. Relationship between *GR* rates and soil texture as a fraction of sand (%), silt (%), and clay (%).

However, *GR* rates are small, and with other factors influencing *GR* rates, it is hard to distinguish the clear relationship between them. According to the Figure 2.8, there are some differences for each texture fraction. For example, trends in *GR* differ between silt and clay at low values of *GR*, while sand fraction role is uncertain.

Overall, interactions of climate, soil, geology, vegetation, land use, and topography are the important factors that control *GR* (Dandekar et al., 2018). The cumulative mean annual *GR* is less than 12 mm in study locations (Figure 2.9).

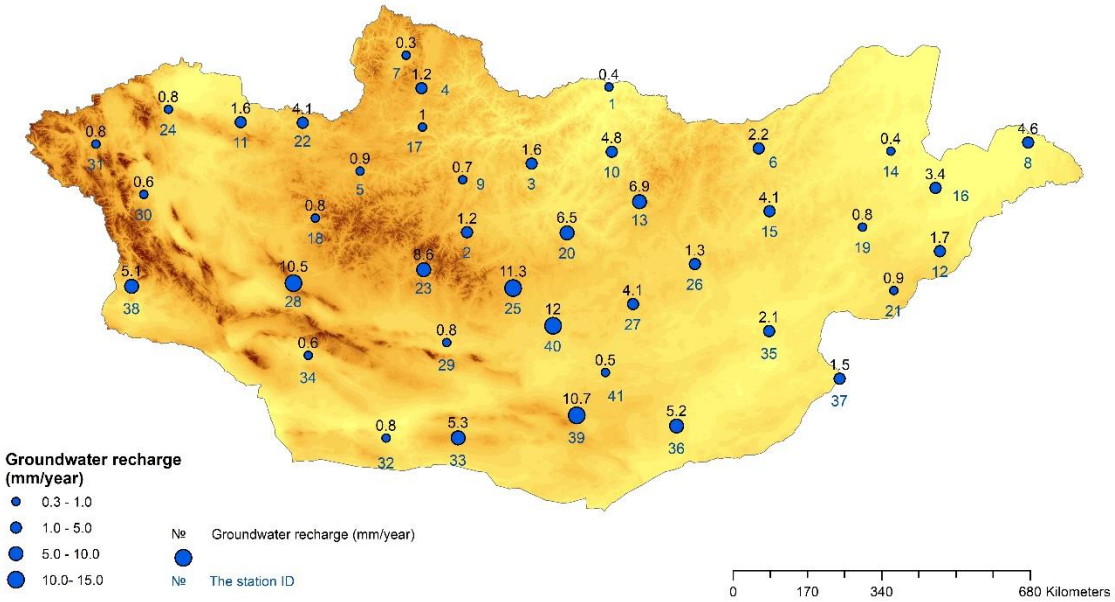

Figure 2.9. The mean annual GR rates in study locations

There is no universal *GR* pattern observed throughout the country; rather, the *GR* in study locations reflect combination of these factors depending on different natural

zones, vegetation, and soil types. The *GR* rates were compared with the map on Figure 2.10 which is used widely in Mongolia (Jadambaa et al., 2012), although with limited description of the methodology. The map is practically the only regional groundwater recharge assessment in Mongolia because it contains groundwater resources, estimated using hydrograph separation. These groundwater resources are naturally the upper limit of the GR, which represents just a fraction of these resources. It is also called "Renewable Groundwater Resource map".

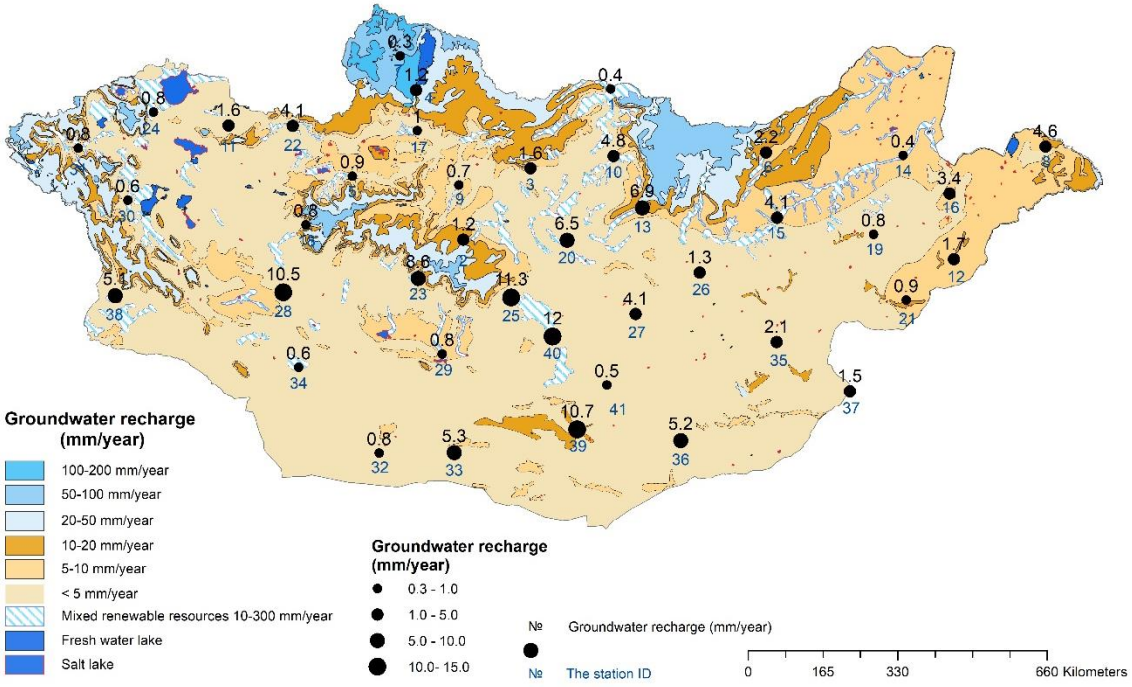

Figure 2.10. Our mean annual *GR* results on the Renewable Groundwater Resource map by (Jadambaa et al., 2012, Figure A1-A80)

According to this map, 76 % of the country has lower than 10 mm/year *GR*, and 84 % of the country has lower than 20 mm/year *GR*. These are areas of desert and steppe. Our mean annual *GR* is lower than 20 mm/year in all study locations and is consistent with the map in most locations. However, it is important to remember that our results

represent the diffused *GR* at the point level, while the map represents both diffused and local *GR*. Thus, the groundwater resources in the map are greater than our simulated *GR* rates. It is apparent that *GR* rates are very variable in large river catchments as well as within the mountain ranges.

Calculating vadose zone lag time

The θ at the bottom of soil profile in HYDRUS-1D can be assumed to be equal to the θ across the bottom soil layer (Z_{bot}) and used to calculate groundwater travel time (Equation 8). The θ at the bottom of the 200 cm soil profile was obtained from the HYDRUS-1D output file at the end of the simulation in all study locations. The travel time in 41 stations has been calculated (Equation 8) with depths to the water table shown in Annex 3.2. The unknown depths to the water table in some locations was replaced with 10 m. The lag time results are shown in Annex 3.3. It can be seen that when the soil is wetter, the depth to the water table is shallower, or when hydraulic conductivity is higher the vadose zone lag time is shorter (Figure 2.11, Annex 3.3).

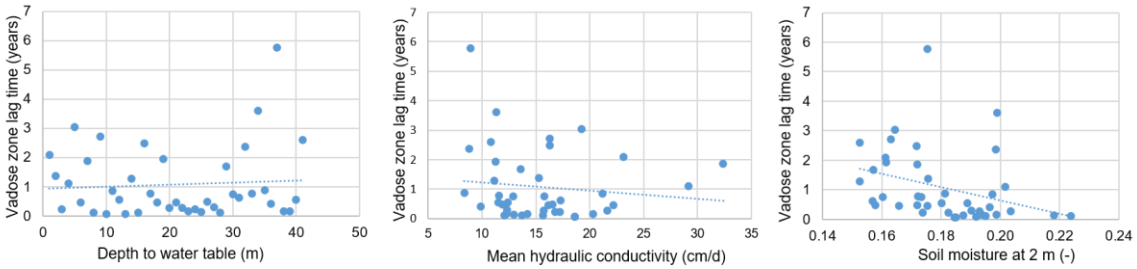

Figure 2.11. Vadose zone lag time vs depth to water table, mean hydraulic conductivity and soil moisture

Conclusions

The *GR* rates were calculated by the vadose zone model HYDRUS-1D in 41 study locations, using climate data for 2007-2011 period. This period provides accurate representation of the various meteorological and vegetation data for entire observation period in each location. The resulting critical input ET_p has been calculated in Chapter 2. Previously *GR* was often neglected in Mongolia or methods failed to consider various factors to *GR*. The study results are site-specific, point results for the diffused *GR*.

In such an arid area, the *GR* rates are very small compared to precipitation in all locations, with an annual mean of less than 12 mm. The inverse relationship between *LAI* and *GR* has been observed, in which the higher *GR* occurs in less vegetated areas. Therefore in two study locations of the Gobi Desert area, smaller *GR* than in other Gobi Desert study locations can be seen due to the saxaul vegetation with deeper roots. The *GR* values in the larger part of the area are consistent with the Renewable Groundwater Resource map, while it shows differences in some river watersheds. This comparison is consistent with total groundwater recharge composition, which includes both diffused and localized recharge.

The study was the first attempt to estimate diffused *GR* in Mongolia with a numerical vadose zone model. The new methodology and data deficiency study may have some uncertainties, which is discussed in the following chapter.

CHAPTER 4. UNCERTAINTY AND CONCLUSIONS

Uncertainty

While different *GR* estimation studies exist in Mongolia, they fail to use recent methodologies, data, or certain hydrologic factors. In some cases, the *GR* is often totally ignored. Thus, it was challenging to use a new method for evaluating *GR* without any previous background knowledge in a less studied arid region. We tried to use methodologies with less data requirements, but required data for the study are unavailable in Mongolia, limited, not in the public domain, or inconsistent. Therefore, our study tried to take advantage of remotely sensed products. Still, some parameters require *in situ* measured data or at least some evaluation of remote sensing data, and replacement methodologies must be implemented. The following identified issues may lead to uncertainties in results, listed in Table 3.1.

Table 3.1. Uncertainties in study

Missing data	Uncertainties	Measurement taken
K_c	There are no available crop coefficients for agricultural crops or natural vegetation in Mongolia.	We proposed the method to develop time-variable K_c in the steppe and implemented K_c method from similar regions in the Gobi Desert area.
LAI in Gobi Desert area	Partitioning ET in Gobi regions lacks reliable *LAI* measurements. Even though some areas are bare and sparsely vegetated, those desert-type areas still had with more bushy type vegetation.	The nearest location with available *LAI* data has been used.
Root water uptake parameters for desert type vegetation	They often have more ability to extract water from drier soils than other vegetation. But the HYDRUS-1D does not offer root water uptake parameters selection for those types of vegetation.	The T_p in the Gobi area constitutes a small portion of total $ET_{p,}$ thus, the overall affect can be small. Even though specific root water uptake parameters for this specific vegetation was not modified, the root depth was changing in HYDRUS-1D
Depth to the groundwater table	Most data are not digitized or available for access. For example, groundwater wells data in some	The groundwater table depth in study locations is obtained from some maps

	cases are considered as state secret information; thus it is hard to obtain the wells data.	approximately, and it may not represent the exact depth to the groundwater table.
Soil hydraulic parameters	There are not any site-specific developed PTFs in Mongolia.	The commonly used Rosetta PTF and VG soil hydraulic model have been used.
Soil temperature data	The soil moisture data can be helpful to optimize the study reliability, or it can be used to calibrate the computations in HYDRUS-1D.	The “spin-up” method has been used to equilibrate soil moisture conditions with atmospheric flux.

The available measurements were accessed to overcome arising issues to the best of our knowledge.

Conclusions

The study has developed the time-variable K_c and calculated ET_p in study locations. With the ET_p and other required data, the numerical vadose zone modeling tool HYDRUS-1D has been used for estimating the diffuse *GR*. Most of the data required for this study have been collected from the remote sensing products, and their reliability was verified by locally measured meteorological data. This practice can be useful in areas with data paucity. The advantage of calculating *GR* with HYDRUS-1D is in its consideration of meteorological, soil, and vegetation processes and parameters; therefore, depending on the site characteristics, various functions of HYDRUS-1D can be used. This aspect is important for understanding various processes of the infiltrating precipitation before soil moisture becomes *GR* in a given location. Method helps to understand *GR* characteristics in different locations with different vegetation types, vegetation cover, precipitation rate, and soil texture.

The mean annual *GR* rates were smaller than 12 mm in study locations. These values were consistent with the groundwater resources maps of Mongolia available from hydrograph separation. Although the diffuse *GR* rates at selected points are small, the total recharge volume over a large area is very significant. Therefore, even such small *GR* rates are important for sustainable water resources management.

This study is the first calculation of ET_p using new crop coefficient in natural vegetated areas with the HYDRUS-1D applications for *GR* estimation. Although the uncertainties of these methodologies in less-studied regions are apparent, further studies can improve the calculation of crop coefficients for natural vegetation conditions throughout the country, including the Gobi Desert plants. The accuracy of the study can

be improved by obtaining missing data listed above. For example, *in situ* studies can be conducted with lysimeters in various settings to estimate the *ET* and *GR*. It is crucial to use hydrologic and vadose zone models and provide better verification in future studies.

References

Adane, Z., Zlotnik, V. A., Rossman, N. R., Wang, T., & Nasta, P. (2019). Sensitivity of potential groundwater recharge to projected climate change scenarios: A site-specific study in the Nebraska Sand Hills, USA. *Water (Switzerland)*, *11*(5). https://doi.org/10.3390/w11050950

Adane, Z. A., Nasta, P., Zlotnik, V., & Wedin, D. (2018). Impact of grassland conversion to forest on groundwater recharge in the Nebraska Sand Hills. *Journal of Hydrology: Regional Studies*, *15*, 171–183. https://doi.org/10.1016/j.ejrh.2018.01.001

Aerogeology Research Institute in Moscow. (1981). *Mongolia Map of multi-annual average runoff in surface and groundwater at scale 1:1.000.000*.

Ajami, H., McCabe, M. F., Evans, J. P., & Stisen, S. (2014). Assessing the impact of model spin-up on surface water-groundwater interactions using an integrated hydrologic model, 5375–5377. https://doi.org/doi:10.1002/2013WR014258.

Allen, R. G. (1998). *Crop evapotranspiration : Guidelines for computing crop water requirements*. FAO of the UN.

Amatya, Skaggs, & Gregory. (1995). Comparison of Methods for Estimating REF-ET. *Journal of Irrigation and Drainage Engineering*, *121*(6), 427–435. https://doi.org/10.1061/(ASCE)0733-9437(1995)121:6(427)

Barnes, C. J., Jacobson, G., & Smith, G. D. (1994). The Distributed Recharge Mechanism in the Australian Arid Zone. *Soil Science Society of America Journal*. https://doi.org/10.2136/sssaj1994.03615995005800010005x

Batkhishig, O., Dolgorsuren, G., Gerelchuluun, J., Puntsagsuren, C., Baldandorj, T., Bron, J., et al. (2013). Integrated Water Management - National Assessment Report Volume I.

Bian, Y., Dai, H., Zhang, Q., Yang, L., & Du, W. (2020). Spatial distribution of potential evapotranspiration trends in the Inner Mongolia Autonomous Region (1971–2016). *Theoretical and Applied Climatology*, *140*(3–4), 1161–1169. https://doi.org/10.1007/s00704-020-03154-y

Blaney, H. F., & Criddle, W. D. (1962). Determining consumptive use and irrigation water requirements. *United States Department of Agriculture*, *Technical*, 1–59.

van den Bosch, R., & Batjes, N, H. (2013). ISRIC - World Soil Information (WDC-Soils). https://doi.org/doi:10.17027/isric-wdcsoils.20200605]

Bouma, J. (1989). Using Soil Survey Data for Quantitative Land Evaluation. https://doi.org/10.1007/978-1-4612-3532-3_4

Celestin, S., Qi, F., Li, R., Yu, T., & Cheng, W. (2020). Evaluation of 32 simple equations against the penman–monteith method to estimate the reference evapotranspiration in the hexi corridor, northwest china. *Water (Switzerland)*, *12*(10). https://doi.org/10.3390/w12102772

Dandekar, A. T., Singh, D. K., Sarangi, A., & Singh, A. K. (2018). Modelling vadose zone processes for assessing groundwater recharge in semi-arid region. *Current Science*, *114*(3), 608–618. https://doi.org/10.18520/cs/v114/i03/608-618

David, F. H., & Vokhmin, V. (2002). THE GLOBAL BIOGEOGRAPHY OF ROOTS. *Journal of Nuclear Science and Technology*, *39*(3), 286–289.

https://doi.org/10.1080/00223131.2002.10875464
Doorenbos, J., & Pruitt, W. O. (1977). Guidelines for predicting crop water requirements. *FAO Irrigation and Drainage Paper*, *24*, 144.
Dorigo, W. A., Wagner, W., Hohensinn, R., Hahn, S., Paulik, C., Xaver, A., et al. (2011). The International Soil Moisture Network: A data hosting facility for global in situ soil moisture measurements. *Hydrology and Earth System Sciences*, *15*(5), 1675–1698. https://doi.org/10.5194/hess-15-1675-2011
Earth Resources Observation And Science center. (2017). Shuttle Radar Topography Mission (SRTM) 3 Arc-Second Global. https://doi.org/https://doi.org/10.5066/F7PR7TFT
FAO-UN. (2015). Global map of aridity. Retrieved November 17, 2020, from http://www.fao.org/geonetwork/srv/en/main.home?uuid=221072ae-2090-48a1-be6f-5a88f061431a
FAO. (2009a). Global map of yearly actual ET.
FAO. (2009b). Global Map of Yearly Crop Reference Evapotranspiration. Retrieved from http://www.fao.org/geonetwork/srv/en/metadata.show?id=7416&currTab=distribution
Gao, F., Feng, G., Ouyang, Y., Wang, H., Fisher, D., Adeli, A., & Jenkins, J. (2017). Evaluation of Reference Evapotranspiration Methods in Arid, Semiarid, and Humid Regions. *Journal of the American Water Resources Association*, *53*(4), 791–808. https://doi.org/10.1111/1752-1688.12530
Gee, G. W., Wierenga, P. J., Andraski, B. J., Young, M. H., Fayer, M. J., & Rockhold, M. L. (1994). Variations in Water Balance and Recharge Potential at Three Western Desert Sites. *Soil Science Society of America Journal*, *58*(1), 63–72. https://doi.org/10.2136/sssaj1994.03615995005800010009x
van Genuchten, M. T. (1980). A Closed-form Equation for Predicting the Hydraulic Conductivity of Unsaturated Soils. *Soil Science Society of America Journal*, *44*(5), 892–898. https://doi.org/10.2136/sssaj1980.03615995004400050002x
Gomariz-Castillo, F., Alonso-Sarría, F., & Cabezas-Calvo-Rubio, F. (2018). Calibration and spatial modelling of daily ET0 in semiarid areas using Hargreaves equation. *Earth Science Informatics*, *11*(3), 325–340. https://doi.org/10.1007/s12145-017-0327-1
Hargreaves, G. H., & Samani, Z. A. (1985). Reference Crop Evapotranspiration From Temperature. *Paper - American Society of Agricultural Engineers*, *4*(May), 96–99. https://doi.org/doi: 10.13031/2013.26773
Indree, T. (2014). *The steppe vegetation of Mongolia*. Ulaanbaatar. Retrieved from https://www.researchgate.net/publication/271448082_The_Steppe_Vegetation_of_Mongolia
J. Šimůnek, M. Šejna, H. Saito, M. Sakai, and M. T. van G. (2008). Version 4.0 April 2008, (April).
Jadambaa, N., Batjargal, D., Linden, W. van der, Batsukh, N., & Borchuluun, U. (2012). *Part 4. Groundwater resources assessment in Integrated Water Management - National Assessment Report Volume I*. Ulaanbaatar. Retrieved from http://bic.iwlearn.org/en/documents/documents/state-reports/2012/integrated-water-management-natioinal-report-volume-i-english/view

Jia, X., Dukes, M. D., & Jacobs, J. M. (2009). Bahiagrass crop coefficients from eddy correlation measurements in central Florida. *Irrigation Science*, *28*(1), 5–15. https://doi.org/10.1007/s00271-009-0176-x

Jyrkama, M. I., Sykes, J. F., & Normani, S. D. (2002). Recharge estimation for transient ground water modeling.

Kjaersgaard, J. H., Plauborg, F., Mollerup, M., Petersen, C. T., & Hansen, S. (2008). Crop coefficients for winter wheat in a sub-humid climate regime. *Agricultural Water Management*, *95*(8), 918–924. https://doi.org/10.1016/j.agwat.2008.03.004

Kukal, M. S., Irmak, S., Walia, H., & Odhiambo, L. (2020). Spatio-temporal calibration of Hargreaves-Samani model to estimate reference evapotranspiration across U.S. High Plains. *Agronomy Journal*, *112*(5), 4232–4248. https://doi.org/10.1002/agj2.20325

Lamchin, M., Park, T., Lee, J. Y., & Lee, W. K. (2015). Monitoring of Vegetation Dynamics in the Mongolia Using MODIS NDVIs and their Relationship to Rainfall by Natural Zone. *Journal of the Indian Society of Remote Sensing*, *43*(2), 325–337. https://doi.org/10.1007/s12524-014-0366-8

Lerner, D., Issar, A. S., & Simmers, I. (1990). Groundwater recharge: A guide to understanding and estimating natural recharge. https://doi.org/https://doi.org/10.2134/jeq1992.00472425002100030036x

Li, S. G., Asanuma, J., Kotani, A., Davaa, G., & Oyunbaatar, D. (2007). Evapotranspiration from a Mongolian steppe under grazing and its environmental constraints. *Journal of Hydrology*, *333*(1), 133–143. https://doi.org/10.1016/j.jhydrol.2006.07.021

Liao, K. H., Xu, S. H., Wu, J. C., Ji, S. H., & Lin, Q. (2011). Assessing Soil Water Retention Characteristics and Their Spatial Variability Using Pedotransfer Functions. *Pedosphere*, *21*(4), 413–422. https://doi.org/10.1016/S1002-0160(11)60143-4

Ma, X., Yasunari, T., Ohata, T., Natsagdorj, L., Davaa, G., & Oyunbaatar, D. (2003). Hydrological regime analysis of the Selenge River basin, Mongolia. *Hydrological Processes*, *17*(14), 2929–2945. https://doi.org/10.1002/hyp.1442

Mao, J., & Yan., B. (2019). Global Monthly Mean Leaf Area Index Climatology, 1981-2015. https://doi.org/10.3334/ORNLDAAC/1653

Menne, M. J., Durre, I., Korzeniewski, B., McNeill, S., & Thomas, K., Yin, X. (2012). Global Historical Climatology Network - Daily (GHCN-Daily), Version 3 [Data set]. https://doi.org/https://doi.org/10.7289/V5D21VHZ

Mineral resources and Petreloum Authority. (1994). Hydrogeology map 1:500000.

Mintz.Y, & Walker.G.K. (1993a). Global fields of Soil Moisture and Land Surface Evapotranspiration Derived from Observed Precipitation and Surface Air Temperature. *Journal of Applied Meteorology*, *32*(8), 1305–1334. https://doi.org/doi.org/10.1175/1520-0450(1993)032<1305:GFOSMA>2.0.CO;2

Mintz.Y, & Walker.G.K. (1993b). Global Fields of Soil Moisture and Land Surface Evapotranspiration Derived from Observed Precipitation and Surface Air Temperature. *Journal of Applied Meteorology*, *32*(8), 1305–1334. https://doi.org/10.1175/1520-0450(1993)032<1305:GFOSMA>2.0.CO;2

Mohawesh, O. E., & Talozi, S. A. (2012). Comparison of Hargreaves and FAO56 equations for estimating monthly evapotranspiration for semi-arid and arid

environments. *Archives of Agronomy and Soil Science*, *58*(3), 321–334. https://doi.org/10.1080/03650340.2010.516253

Mualem, Y. (1976). A New Model for Predicting the Hydaulic Conductivity of Unsaturated Porous Media. *Water Resources Research*, *12*(3).

Nandintsetseg, B., & Shinoda, M. (2011). Seasonal change of soil moisture in Mongolia: Its climatology and modelling. *International Journal of Climatology*, *31*(8), 1143–1152. https://doi.org/10.1002/joc.2134

Nandintsetseg, B., & Shinoda, M. (2014). Multi-Decadal Soil Moisture Trends in Mongolia and Their Relationships to Precipitation and Evapotranspiration. *Arid Land Research and Management*, *28*(3), 247–260. https://doi.org/10.1080/15324982.2013.861882

Nasta, P., & Gates, J. B. (2013). Plot-scale modeling of soil water dynamics and impacts of drought conditions beneath rainfed maize in Eastern Nebraska. *Agricultural Water Management*, *128*(December 2012), 120–130. https://doi.org/10.1016/j.agwat.2013.06.021

National Agency for Meteorology and Environmental Monitoring. (n.d.). Precipitation. Retrieved from http://tsag-agaar.gov.mn/

Natsagdorj, E., Renchin, T., De Maeyer, P., Tseveen, B., Dari, C., & Dashdondog, E. (2019). SOIL MOISTURE ANALYSIS USING MULTISPECTRAL DATA in NORTH CENTRAL PART of Mongolia. *ISPRS Annals of the Photogrammetry, Remote Sensing and Spatial Information Sciences*, *4*(2/W5), 485–491. https://doi.org/10.5194/isprs-annals-IV-2-W5-485-2019

P.Khishigsuren, & Linden, W. van der. (2012). *Part 2. Land use Integrated Water Management - National Assessment Report Volume I*. Ulaanbaatar. Retrieved from http://bic.iwlearn.org/en/documents/documents/state-reports/2012/integrated-water-management-natioinal-report-volume-i-english/view

Patricia, G. M. H., Jeffrey, P. L. W., Raffensperger, G. M. H. P. L. W. J. P., & D'Odorico, P. (2015). Elements of Physical Hydrology, 2nd Edition. *Groundwater*, *53*(4), 509–510. https://doi.org/10.1111/gwat.12343

Pelosi, A., Medina, H., Villani, P., D'Urso, G., & Chirico, G. B. (2016). Probabilistic forecasting of reference evapotranspiration with a limited area ensemble prediction system. *Agricultural Water Management*, *178*, 106–118. https://doi.org/10.1016/j.agwat.2016.09.015

Pockman, W., & Sperry, J. (2000). Vulnerability to Xylem Cavitation and the Distribution of Sonoran Desert Vegetation. *American Journal of Botany*, *87*, 1287–1299. https://doi.org/10.2307/2656722

Prych, E. A. (1998). Using chloride and chlorine-36 as soil-water tracers to estimate deep percolation at selected locations on the US Department of Energy Hanford Site, Washington. US Geological Survey.

R.A.Feddes. (1978). Simulation of Field Water Use and Crop Yield. *Soil Science*, *129*(3), 193. https://doi.org/10.1097/00010694-198003000-00016

Radcliffe, D.E. and Simunek, J. (2010). Soil Physics with Hydrus: Modeling and Applications.

Ritchie, J. T. (1972). Model for predicting evaporation from a row crop with incomplete cover. *Water Resources Research*, *8*(5), 1204–1213. https://doi.org/10.1029/WR008i005p01204

Robock, A., Vinnikov, K. Y., Srinivasan, G., Entin, J. K., Hollinger, S. E., Speranskaya, N. A., et al. (2000). The Global Soil Moisture Data Bank. *Bulletin of the American Meteorological Society*, *81*(6), 1281–1299. https://doi.org/10.1175/1520-0477(2000)081<1281:TGSMDB>2.3.CO;2

Rockhold, M. L., Fayer, M. J., Kincaid, C. T., & Gee, G. W. (1995). Estimation of natural ground water recharge for the performance assessment of a low-level waste disposal facility at the Hanford site, (March), 93. Retrieved from https://www.osti.gov/biblio/46664%0Ahttp://inis.iaea.org/search/search.aspx?orig_q=RN:26060572

Romanova, Mosolova, & Beresneva. (1983). Microclimatology and Its Significance for Agriculture. *Gidrometeoizdat*.

Rossman, N. R., Zlotnik, V. A., Rowe, C. M., & Szilagyi, J. (2014). Vadose zone lag time and potential 21st century climate change effects on spatially distributed groundwater recharge in the semi-arid Nebraska Sand Hills. *Journal of Hydrology*, *519*, 656–669. https://doi.org/10.1016/j.jhydrol.2014.07.057

Scanlon, B. R., Healy, R. W., & Cook, P. G. (2002). Choosing appropriate techniques for quantifying groundwater recharge, (February). https://doi.org/10.1007/s10040-0010176-2

Schaap, M. G., Leij, F. J., & Van Genuchten, M. T. (2001). Rosetta: A computer program for estimating soil hydraulic parameters with hierarchical pedotransfer functions. *Journal of Hydrology*, *251*(3–4), 163–176. https://doi.org/10.1016/S0022-1694(01)00466-8

Šimunek, J. (2015). Estimating groundwater recharge using HYDRUS-1D, 25–36.

Small, E. E. (2005). Climatic controls on diffuse groundwater recharge in semiarid environments of the southwestern United States. *Water Resources Research*, *41*(4), 1–17. https://doi.org/10.1029/2004WR003193

Spinoni, J., Vogt, J., Naumann, G., Carrao, H., & Barbosa, P. (2015). Towards identifying areas at climatological risk of desertification using the Köppen-Geiger classification and FAO aridity index. *International Journal of Climatology*, *35*(9), 2210–2222. https://doi.org/10.1002/joc.4124

Stephens, D. B. (1994). A Perspective on Diffuse Natural Recharge Mechanisms in Areas of Low Precipitation. *Soil Science Society of America Journal*. https://doi.org/10.2136/sssaj1994.03615995005800010006x

Suleiman, A. A., Tojo Soler, C. M., & Hoogenboom, G. (2007). Evaluation of FAO-56 crop coefficient procedures for deficit irrigation management of cotton in a humid climate. *Agricultural Water Management*, *91*(1–3), 33–42. https://doi.org/10.1016/j.agwat.2007.03.006

Sumner, D. M., & Jacobs, J. M. (2005). Utility of Penman-Monteith, Priestley-Taylor, reference evapotranspiration, and pan evaporation methods to estimate pasture evapotranspiration. *Journal of Hydrology*, *308*(1–4), 81–104. https://doi.org/10.1016/j.jhydrol.2004.10.023

Suyker, A. E., & Verma, S. B. (2009). Evapotranspiration of irrigated and rainfed maize-soybean cropping systems. *Agricultural and Forest Meteorology*, *149*(3–4), 443–452. https://doi.org/10.1016/j.agrformet.2008.09.010

Tabari, H., & Talaee, P. H. (2011). Local Calibration of the Hargreaves and Priestley-Taylor Equations for Estimating Reference Evapotranspiration in Arid and Cold

Climates of Iran Based on the Penman-Monteith Model. *Journal of Hydrologic Engineering*, *16*(10), 837–845. https://doi.org/10.1061/(asce)he.1943-5584.0000366

Thornthwaite, C. W. (1948). An Approach toward a Rational Classification of Climate. *Geographical Review*, *38*(1), 55. https://doi.org/10.2307/210739

Wang, K., Wang, P., Li, Z., Cribb, M., & Sparrow, M. (2007). A simple method to estimate actual evapotranspiration from a combination of net radiation, vegetation index, and temperature. *Journal of Geophysical Research Atmospheres*, *112*(15), 1–14. https://doi.org/10.1029/2006JD008351

Wang, T., Zlotnik, V. A., Šimunek, J., & Schaap, M. G. (2009). Using pedotransfer functions in vadose zone models for estimating groundwater recharge in semiarid regions. *Water Resources Research*, *45*(4), 1–12. https://doi.org/10.1029/2008WR006903

Wang, Z. Y., Hou, J., Qu, Z. Q., Guo, J. Y., & Li, J. R. (2017). Root distribution of 430 plants in temperate grassland of northern China. *Applied Ecology and Environmental Research*, *15*(3), 1625–1651. https://doi.org/10.15666/aeer/1503_16251651

WeatherOnline Ltd. (2021). Weather Online website. Retrieved October 10, 2020, from https://www.weatheronline.co.uk/weather/maps/forecastmaps?LANG=en&CONT=asie&REGION=0026&LAND=VM&UP=1&R=0&CEL=C

Wösten, J. H. M., Pachepsky, Y. A., & Rawls, W. J. (2001). Pedotransfer functions: Bridging the gap between available basic soil data and missing soil hydraulic characteristics. *Journal of Hydrology*, *251*(3–4), 123–150. https://doi.org/10.1016/S0022-1694(01)00464-4

Xia, J., Liang, S., Chen, J., Yuan, W., Liu, S., Li, L., et al. (2014). Satellite-based analysis of evapotranspiration and water balance in the grassland ecosystems of Dryland East Asia. *PLoS ONE*, *9*(5). https://doi.org/10.1371/journal.pone.0097295

Xiang, K., Li, Y., Horton, R., & Feng, H. (2020). Similarity and difference of potential evapotranspiration and reference crop evapotranspiration – a review. *Agricultural Water Management*, *232*(January). https://doi.org/10.1016/j.agwat.2020.106043

Xu, C. Y., & Singh, V. P. (2002). Cross comparison of empirical equations for calculating potential evapotranspiration with data from Switzerland. *Water Resources Management*, *16*(3), 197–219. https://doi.org/10.1023/A:1020282515975

Yanagawa, A., Fujimaki, H., Okuro, T., Jamsran, U., & Takeuchi, K. (2015). Comparison of drought tolerances in a root water uptake model for two co-occurring grass species in Mongolia. *J. Jpn. Soc. Soil Phys. No*, *130*(130), 3–10. Retrieved from https://js-soilphysics.com/downloads/pdf/130003.pdf

Yang, F., & Zhou, G. (2011). Characteristics and modeling of evapotranspiration over a temperate desert steppe in Inner Mongolia, China. *Journal of Hydrology*, *396*(1–2), 139–147. https://doi.org/10.1016/j.jhydrol.2010.11.001

Yu, D., Yang, J., Shi, L., Zhang, Q., Huang, K., Fang, Y., & Zha, Y. (2019). On the uncertainty of initial condition and initialization approaches in variably saturated flow modeling. *Hydrology and Earth System Sciences*, *23*(7), 2897–2914. https://doi.org/10.5194/hess-23-2897-2019

Yu, W., Wu, T., Wang, W., Li, R., Wang, T., Qin, Y., et al. (2016). Spatiotemporal Changes of Reference Evapotranspiration in Mongolia during 1980-2006. *Advances in Meteorology*, *2016*. https://doi.org/10.1155/2016/9586896

Zeng, W. Z., Lei, G. Q., Zhang, H. Y., Hong, M. H., Xu, C., Wu, J. W., & Huang, J. S. (2017). Estimating Root Zone Moisture from Surface Soil Using Limited Data. *Ecological Chemistry and Engineering S*, *24*(4), 501–516. https://doi.org/10.1515/eces-2017-0033

Zhang, F., Zhou, G., Wang, Y., Yang, F., & Nilsson, C. (2012). Evapotranspiration and crop coefficient for a temperate desert steppe ecosystem using eddy covariance in Inner Mongolia, China. *Hydrological Processes*, *26*(3), 379–386. https://doi.org/10.1002/hyp.8136

Zhang, Yinsheng, Munkhtsetseg, E., Kadota, T., & Ohata, T. (2005). An observational study of ecohydrology of a sparse grassland at the edge of the Eurasian cryosphere in Mongolia. *Journal of Geophysical Research D: Atmospheres*, *110*(14), 1–14. https://doi.org/10.1029/2004JD005474

Zhang, Yonggen, & Schaap, M. G. (2017a). Weighted recalibration of the Rosetta pedotransfer model with improved estimates of hydraulic parameter distributions and summary statistics (Rosetta3). *Journal of Hydrology*, *547*, 39–53. https://doi.org/10.1016/j.jhydrol.2017.01.004

Zhang, Yonggen, & Schaap, M. G. (2017b). Weighted recalibration of the Rosetta pedotransfer model with improved estimates of hydraulic parameter distributions and summary statistics (Rosetta3). *Journal of Hydrology*, *547*(January 2017), 39–53. https://doi.org/10.1016/j.jhydrol.2017.01.004

Zorigt, M., Linden, W. van der, & G, D. (2012). *Part 2. Integrated Water Management - National Assessment Report Volume I*. Ulaanbaatar. Retrieved from http://bic.iwlearn.org/en/documents/documents/state-reports/2012/integrated-water-management-natioinal-report-volume-i-english/view

Appendices

CHAPTER 2. SELECTION OF EVAPOTRANSPIRATION METHOD

Annex 2.1. LAI values at study locations

№	Stations / LAI	Average LAI	Jan	Feb	Mar	Apr	May	Jun	Jul	Aug	Sep	Oct	Nov	Dec
1	Sukhbaatar	0.98	0.27	0.22	0.32	0.59	1.29	1.96	1.70	2.02	1.80	0.69	0.40	0.43
2	Tseterleg	0.86	0.20	0.13	0.19	0.29	0.74	1.79	2.54	2.44	1.35	0.32	0.21	0.12
3	Bulgan Mg	0.86	0.19	0.11	0.20	0.30	0.46	0.93	1.36	1.31	0.89	0.33	0.22	0.13
4	Khatgal	0.64	0.17	0.10	0.14	0.27	0.47	1.22	1.91	1.79	0.96	0.28	0.18	0.12
5	Tosontsengel	0.63	0.15	0.10	0.05	0.24	0.61	1.46	1.81	1.66	0.93	0.30	0.14	0.11
6	Binder	0.62	0.16	0.11	0.16	0.30	0.60	1.00	1.69	1.77	1.06	0.31	0.17	0.13
7	Rinchinlhumbe	0.60	0.15	0.10	0.08	0.25	0.58	1.23	1.70	1.59	0.90	0.31	0.15	0.11
8	Khalkh gol	0.56	0.16	0.10	0.10	0.30	0.55	0.85	1.48	1.55	0.99	0.31	0.17	0.11
9	Erdenemandal	0.52	0.17	0.11	0.17	0.23	0.46	0.96	1.40	1.30	0.80	0.27	0.18	0.12
10	Baruunkharaa	0.52	0.16	0.09	0.17	0.30	0.46	0.88	1.28	1.29	0.92	0.35	0.19	0.11
11	Baruunturuun	0.50	0.16	0.10	0.07	0.32	0.61	1.04	1.02	1.12	0.76	0.42	0.22	0.11
12	Erdenetsagaan	0.49	0.18	0.11	0.14	0.32	0.45	0.74	1.16	1.27	0.77	0.35	0.23	0.12
13	Chingis khaan (UB)	0.42	0.18	0.11	0.14	0.26	0.45	0.77	1.00	0.97	0.60	0.25	0.15	0.11
14	Choibalsan	0.41	0.17	0.11	0.15	0.30	0.36	0.56	0.89	1.06	0.66	0.30	0.19	0.12
15	Undurkhaan	0.40	0.17	0.11	0.16	0.30	0.36	0.58	0.83	1.00	0.62	0.30	0.19	0.12
16	Matad	0.39	0.17	0.10	0.11	0.28	0.47	0.55	0.81	0.96	0.62	0.28	0.15	0.11
17	Murun	0.39	0.17	0.11	0.15	0.20	0.28	0.68	0.95	1.01	0.51	0.25	0.18	0.13
18	Uliastai	0.38	0.17	0.10	0.07	0.25	0.32	0.73	0.91	0.88	0.49	0.33	0.18	0.10
19	Baruun-Urt	0.38	0.18	0.11	0.17	0.30	0.32	0.38	0.79	0.94	0.61	0.31	0.24	0.13
20	Erdenesant	0.34	0.17	0.11	0.16	0.24	0.33	0.51	0.70	0.85	0.52	0.27	0.15	0.10
21	Dariganga	0.32	0.15	0.10	0.12	0.31	0.29	0.36	0.65	0.85	0.46	0.29	0.19	0.11

22	Baynuul	0.31	0.12	0.10	0.04	0.18	0.32	0.59	0.66	0.74	0.40	0.25	0.15	0.11
23	Galuut	0.28	0.16	0.10	0.11	0.20	0.22	0.36	0.60	0.73	0.36	0.23	0.14	0.10
24	Ulaangom	0.26	0.14	0.10	0.04	0.19	0.34	0.38	0.49	0.59	0.34	0.26	0.16	0.10
25	Arvaikheer	0.24	0.18	0.10	0.06	0.13	0.21	0.23	0.55	0.71	0.38	0.20	0.07	0.10
26	Choir	0.24	0.15	0.10	0.13	0.22	0.21	0.34	0.46	0.63	0.31	0.23	0.14	0.10
27	Mandalgobi	0.20	0.18	0.10	0.11	0.20	0.20	0.30	0.40	0.50	0.22	0.21	0.11	0.10
28	Altai	0.20	0.16	0.10	0.10	0.17	0.21	0.31	0.41	0.50	0.22	0.20	0.08	0.10
29	Khoriult	0.21	0.15	0.10	0.08	0.18	0.20	0.31	0.42	0.49	0.19	0.20	0.09	0.10
30	Hovd	0.21	0.17	0.10	0.09	0.12	0.22	0.25	0.44	0.52	0.25	0.19	0.09	0.10
31	Ulgii	0.23	0.18	0.10	0.11	0.12	0.29	0.37	0.45	0.50	0.14	0.20	0.13	0.11
32	Ekhiingol	0.21	0.15	0.10	0.08	0.18	0.20	0.31	0.42	0.49	0.19	0.20	0.09	0.10
33	Gurvantes	0.21	0.15	0.10	0.08	0.18	0.20	0.31	0.42	0.49	0.19	0.20	0.09	0.10
34	Tooroi	0.22	0.16	0.10	0.10	0.17	0.21	0.31	0.41	0.50	0.22	0.20	0.08	0.10
35	Sainshand	0.18	0.15	0.10	0.09	0.20	0.20	0.26	0.31	0.35	0.10	0.19	0.07	0.10
36	Khanbogd	0.17	0.17	0.10	0.09	0.20	0.20	0.25	0.30	0.33	0.09	0.20	0.06	0.10
37	Zamiin Uud	0.17	0.17	0.10	0.09	0.20	0.20	0.25	0.30	0.33	0.09	0.20	0.06	0.10
38	Baitag	0.15	0.10	0.10	0.05	0.10	0.28	0.28	0.27	0.25	0.01	0.20	0.04	0.10
39	Dalanzadgad	0.14	0.12	0.10	0.05	0.17	0.29	0.24	0.20	0.20	0.02	0.18	0.02	0.10
40	Saikhan-Ovoo	0.14	0.12	0.10	0.05	0.17	0.29	0.24	0.20	0.20	0.02	0.18	0.02	0.10
41	Tsogt-Ovoo	0.14	0.12	0.10	0.05	0.17	0.29	0.24	0.20	0.20	0.02	0.18	0.02	0.10

CHAPTER 3. THE ANALYSIS OF GROUNDWATER RECHARGE

Annex 3.1. The soil moisture at test locations

Stations	Depth (cm)	θ									
		0-10	10-20	20-30	30-40	40-50	50-60	60-70	70-80	80-90	90-100
1. Galuut	Avg	0.22	0.22	0.21	0.23	0.24	0.25	0.25	0.26	0.26	0.26
	Max	0.38	0.37	0.37	0.41	0.42	0.41	0.40	0.44	0.45	0.50
	Min	0.16	0.16	0.15	0.18	0.18	0.19	0.19	0.20	0.19	0.20
2.Tsetserleg	Avg	0.19	0.16	0.17	0.20	0.20	0.20	0.18	0.17	0.17	0.16
	Max	0.38	0.32	0.41	0.35	0.38	0.38	0.27	0.26	0.26	0.23
	Min	0.09	0.07	0.08	0.09	0.08	0.10	0.10	0.10	0.11	0.09
3.Bulgan	Avg	0.38	0.36	0.36	0.36	0.38	0.40	0.39	0.39	0.40	0.40
	Max	0.61	0.67	0.63	0.58	0.63	0.67	0.63	0.64	0.67	0.64
	Min	0.27	0.26	0.25	0.25	0.26	0.27	0.26	0.27	0.26	0.26
4.Khovd	Avg	0.22	0.22	0.22	0.19	0.19	0.19	0.19	0.19	0.19	0.19
	Max	0.30	0.33	0.33	0.34	0.29	0.28	0.33	0.38	0.34	0.35
	Min	0.18	0.18	0.18	0.15	0.15	0.15	0.15	0.15	0.15	0.15
5.Erdenetsagaan	Avg	0.27	0.27	0.28	0.29	0.30	0.31	0.31	0.32	0.32	0.32
	Max	0.43	0.44	0.45	0.43	0.48	0.50	0.49	0.61	0.58	0.58
	Min	0.20	0.20	0.21	0.23	0.23	0.24	0.25	0.26	0.25	0.24
6.Choibalsan	Avg	0.22	0.22	0.22	0.24	0.24	0.24	0.25	0.25	0.25	0.25
	Max	0.32	0.32	0.35	0.37	0.37	0.37	0.40	0.40	0.40	0.38
	Min	0.18	0.17	0.18	0.19	0.19	0.19	0.19	0.18	0.18	0.18
7.Khatgal	Avg	0.26	0.27	0.28	0.29	0.28	0.28	0.25	0.24	0.31	0.27
	Max	0.48	0.43	0.44	0.49	0.43	0.45	0.40	0.41	0.50	0.43
	Min	0.13	0.13	0.12	0.14	0.14	0.15	0.11	0.13	0.18	0.16
8.Baruunurt	Avg	0.27	0.27	0.28	0.29	0.30	0.31	0.31	0.32	0.32	0.32
	Max	0.43	0.44	0.45	0.43	0.48	0.50	0.49	0.61	0.58	0.58
	Min	0.20	0.20	0.21	0.23	0.23	0.24	0.25	0.26	0.25	0.24
9.Undurkhaan	Avg	0.29	0.29	0.33	0.34	0.33	0.32	0.31	0.32	0.37	0.33
	Max	0.41	0.53	0.57	0.57	0.47	0.41	0.37	0.40	0.46	0.37
	Min	0.22	0.23	0.23	0.26	0.24	0.26	0.26	0.26	0.31	0.29
10. Tsogt-ovoo	Avg	0.19	0.17	0.14	0.19	0.19	0.19	0.18	0.19	0.19	0.20
	Max	0.41	0.34	0.34	0.37	0.39	0.36	0.36	0.36	0.42	0.43
	Min	0.11	0.10	0.07	0.13	0.13	0.12	0.11	0.12	0.12	0.14

Annex 3.2. Depth to the water table in study locations

ID	Stations	D_{wt} (m)	D_{rz} (m)	Z_{bot} (m)
1	Sukhbaatar	12	0.3	11.7
2	Tseterleg	25	0.3	24.7
3	Bulgan Mg	6	0.3	5.7
4	Khatgal	30	0.3	29.7
5	Tosontsengel	30	0.3	29.7
6	Binder	15	0.3	14.7
7	Rinchinlhumbe	7.5	0.3	7.2
8	Khalkh gol	5	0.3	4.7
9	Erdenemandal	20	0.3	19.7
10	Baruunkharaa	5	0.3	4.7
11	Baruunturuun	30	0.3	29.7
12	Erdenetsagaan	8	0.3	7.7
13	Chingis khaan (UB)	5	0.3	4.7
14	Choibalsan	5	0.3	4.7
15	Undurkhaan	5	0.3	4.7
16	Matad	30	0.3	29.7
17	Murun	5	0.3	4.7
18	Uliastai	5	0.3	4.7
19	Baruun-Urt	7.5	0.3	7.2
20	Erdenesant	31	0.3	30.7
21	Dariganga	5	0.3	4.7
22	Baynuul	15	0.3	14.7
23	Galuut	15	0.3	14.7
24	Ulaangom	5	0.3	4.7
25	Arvaikheer	15	0.3	14.7
26	Choir	5	0.3	4.7
27	Mandalgobi	15	0.3	14.7
28	Altai	15	0.3	14.7
29	Khoriult	15	0.3	14.7
30	Hovd	5	0.3	4.7
31	Ulgii	5	0.3	4.7
32	Ekhiingol	15	0.97	14.0
33	Gurvantes	15	0.3	14.7
34	Tooroi	15	0.97	14.0
35	Sainshand	15	0.3	14.7
36	Khanbogd	15	0.3	14.7
37	Zamiin Uud	52	0.3	51.7
38	Baitag	5	0.3	4.7
39	Dalanzadgad	15	0.3	14.7
40	Saikhan-Ovoo	15	0.3	14.7
41	Tsogt-Ovoo	10	0.3	9.7

Annex 3.3. Travel time to groundwater table

ID	Stations	Z_{bot} (m)	θ at 2m (-)	Mean K_s (cm/day)	Days	Years
1	Sukhbaatar	11.7	0.16	23	762.52	2.09
2	Tseterleg	24.7	0.18	15	499.17	1.37
3	Bulgan Mg	5.7	0.17	17	86.63	0.24
4	Khatgal	29.7	0.20	29	403.23	1.10
5	Tosontsengel	29.7	0.16	19	1106.83	3.03
6	Binder	14.7	0.18	22	163.72	0.45
7	Rinchinlhumbe	7.2	0.17	32	682.47	1.87
8	Khalkh gol	4.7	0.19	16	36.62	0.10
9	Erdenemandal	19.7	0.16	16	990.04	2.71
10	Baruunkharaa	4.7	0.18	19	25.70	0.07
11	Baruunturuun	29.7	0.20	21	311.69	0.85
12	Erdenetsagaan	7.7	0.19	12	201.46	0.55
13	Chingis khaan (UB)	4.7	0.18	19	25.25	0.07
14	Choibalsan	4.7	0.15	11	465.68	1.28
15	Undurkhaan	4.7	0.20	12	41.38	0.11
16	Matad	29.7	0.17	16	906.57	2.48
17	Murun	4.7	0.17	16	275.80	0.76
18	Uliastai	4.7	0.16	17	171.95	0.47
19	Baruun-Urt	7.2	0.16	11	707.92	1.94
20	Erdenesant	30.7	0.20	16	97.99	0.27
21	Dariganga	4.7	0.17	16	165.61	0.45
22	Baynuul	14.7	0.19	22	96.16	0.26
23	Galuut	14.7	0.20	20	59.56	0.16
24	Ulaangom	4.7	0.18	17	84.65	0.23
25	Arvaikheer	14.7	0.22	13	46.01	0.13
26	Choir	4.7	0.17	12	172.67	0.47
27	Mandalgobi	14.7	0.19	12	109.36	0.30
28	Altai	14.7	0.22	14	40.79	0.11
29	Khoriult	14.7	0.16	14	614.48	1.68
30	Hovd	4.7	0.16	13	273.21	0.75
31	Ulgii	4.7	0.16	17	225.82	0.62
32	Ekhiingol	14.0	0.20	9	864.97	2.37
33	Gurvantes	14.7	0.17	12	282.00	0.77
34	Tooroi	14.0	0.20	11	1314.84	3.60
35	Sainshand	14.7	0.18	8	317.80	0.87
36	Khanbogd	14.7	0.20	10	147.81	0.40
37	Zamiin Uud	51.7	0.18	9	2105.13	5.77
38	Baitag	4.7	0.19	12	53.27	0.15
39	Dalanzadgad	14.7	0.19	14	61.13	0.17
40	Saikhan-Ovoo	14.7	0.18	11	197.96	0.54
41	Tsogt-Ovoo	9.7	0.15	11	945.61	2.59